



UPPSALA  
UNIVERSITET

UPTEC W13013

Examensarbete 30 hp  
Juni 2013

# Implementation of temperature variations and free surface evolution in the Shallow Ice Approximation (SIA)

---

Cecilia Hård

## Abstract

Ice sheets and glaciers constitute an enormous water storage, currently corresponding to a potential sea level rise of almost 70 meters if all ice was to melt completely. The ice sheets are dynamic components of the global climate system and numerical modeling is a useful tool that can help us understand and predict how the ice sheets develop. The most accurate model available for ice sheets is given by the Stokes equations, but to solve them for a real ice sheet on a relevant time scale would be way too computationally costly. Instead approximations of the Stokes equations are used such as the Shallow Ice Approximation (SIA). The SIA is valid for areas where the aspect ratio  $\epsilon$ , the ice thickness divided by the horizontal extent of the ice, is small.

In this project equations for temperature and surface evolution were implemented in a Matlab version of SIA. The model already had algorithms implemented for computation of stresses, velocities and pressures for an ice sheet with fixed geometry and temperature. Implementation of temperature and free surface equations also made the problem time-dependent.

The result was evaluated by solving a simple test problem and comparing the solution to a full Stokes solution obtained with the code ElmerIce. The SIA solution was closer to the Stokes solution when the aspect ratio  $\epsilon$  and slope  $\alpha$  were decreased simultaneously such that  $\alpha = \arctan \epsilon$ , but a similar improvement was also obtained when only the slope was decreased. The differences between the two solutions were satisfyingly small for both temperature, surface location and velocities for an aspect ratio of  $\epsilon = 7.8 * 10^{-4}$  and  $\alpha = \arctan \epsilon$ .

## Referat

Inlandsisar och glaciärer utgör ett enormt vattenförråd som i dagsläget motsvarar en potentiell havsnivåhöjning på nästan 70 meter om all is skulle smälta helt. Inlandsisarna är en dynamisk del av det globala klimatsystemet och numerisk modellering är ett användbart hjälpmedel för att kunna förstå och förutspå hur inlandsisarna utvecklas. Den bästa tillgängliga modellen för inlandsis utgörs av Stokes ekvationer, men att lösa dem för en riktig inlandsis på en relevant tidsskala skulle vara alldeles för dyrt beräkningsmässigt. I stället används approximationer av Stokes ekvationer som exempelvis Shallow Ice Approximation (SIA). SIA fungerar för områden där kvoten mellan isens tjocklek och dess horisontella utbredning ( $\epsilon$ ) är liten.

I det här projektet har ekvationer för temperatur och isytans förändring implementerats i en Matlab-version av SIA som dessförinnan beräknade spänningar, hastigheter och tryck för en inlandsis med fast geometri och temperatur. Implementering av dessa ekvationer medförde också att problemet blev tidsberoende.

Resultatet utvärderades genom att ett enkelt testproblem löstes och resultatet jämfördes med en Stokes-lösning som beräknats med koden ElmerIce. SIA-lösningen låg närmare Stokes-lösningen då  $\epsilon$  och lutningen  $\alpha$  minskades samtidigt så att förhållandet  $\alpha = \arctan \epsilon$  upprätthölls, men en likvärdig förbättring uppnåddes även då endast lutningen minskades. Skillnaden mellan de båda lösningarna var tillfredställande liten för både temperatur, isytans position och hastigheter för  $\epsilon = 7.8 * 10^{-4}$  och  $\alpha = \arctan \epsilon$ .

# Förord

Detta examensarbete utgör den avslutande delen på civilingenjörsprogrammet i miljö- och vattenteknik vid Uppsala universitet. Arbetet omfattar 30 högskolepoäng och har utförts på avdelningen för beräkningsvetenskap vid institutionen för informationsteknologi. Jag vill tacka min handledare Lina von Sydow och min ämnesgranskare Michael Thuné för stöd och vägledning under arbetet, samt även Josefin Ahlkrona och Per Lötstedt för värdefull hjälp och kommentarer.

Cecilia Håård

Uppsala, juni 2013

## Populärvetenskaplig sammanfattning

I detta projekt har en befintlig modell för simulering av inlandsisar vidareutvecklats från att enbart beräkna isens tryck och rörelser för en fast geometri till att även beräkna temperaturförändringar och ändringar av isens form över tiden.

Inlandsisar och glaciärer är viktiga delar i det globala klimatsystemet, bland annat eftersom de reflekterar solinstrålning och på så vis sänker jordens temperatur. Om isarna minskar i utbredning innebär det att en större del av solenergin hålls kvar i atmosfären och temperaturen stiger, vilket i sin tur kan få isarna att smälta ännu mer. Isarna fyller också en funktion som vattenreservoarer och ändringar i deras utbredning påverkar havsnivån. Den vattenmassa som idag finns lagrad i glaciärer och inlandsisar motsvarar en potentiell havsnivåhöjning på ca 70 meter.

För att en is ska räknas som en glaciär krävs att det ackumulerats så mycket is att den börjar röra sig på grund av sin egen tyngd. Snöfall bygger på ismassan ovanifrån och omvandlas till is när den packas och pressas samman. Isen rör sig långsamt från toppen nedåt och ut mot kanterna där den smälter eller kalvar i havet. En inlandsis är en glaciär vars yta överstiger 50 000 m<sup>2</sup>. I dagsläget finns två inlandsisar på jorden, en på Grönland och en på Antarktis.

Klimatmodellering används dels för att förstå vilka processer som påverkar klimatet och hur klimatet sett ut historiskt på jorden och dels för att kunna förutspå hur klimatet kommer att utvecklas i framtiden. Sådan information är relevant för i stort sett all samhällsplanering över hela världen. Det globala klimatsystemet består av många komponenter, exempelvis atmosfären, haven och inlandsisarna. För var och en av dessa försöker man göra en matematisk beskrivning som sedan kan implementeras i en datormodell som räknar ut vad som händer i olika scenarier.

Den matematiska beskrivningen av en is grundas på att man gör vissa antaganden och bortser från sådant som anses försumbart och är därför alltid en förenkling av verkligheten. När den matematiska modellen sedan ska implementeras i en dator kommer ytterligare begränsningar in i bilden, främst på grund av att ekvationerna måste diskretiseras. Behovet av diskretisering kommer av att datorer har begränsat lagringsutrymme och dessutom kan utföra ett begränsat antal beräkningar per tidsenhet. Därmed är det till exempel inte möjligt att beskriva *alla* punkter i isen - man måste alltid välja ett ändligt antal punkter. Hur många punkter man kan välja och därmed hur tätt de ligger beror av datorns lagringsutrymme och processor samt av hur lång tidsperiod (och hur stor is) man vill simulera. Ju tätare beräkningspunkterna ligger desto bättre blir lösningens noggrannhet.

En inlandsis består generellt sett av två olika typer av is, kall och tempererad. Den kalla isen har en variabel temperatur under isens smältpunkt och en temperaturändring påverkar bland annat viskositeten. Den tempererade isens temperatur är densamma som smältpunkten och den består ofta av en blandning av is och vatten. Om energi tillförs i form av värme till tempererad is ändras inte temperaturen utan bara förhållandet mellan is och vatten eftersom mer av isen kommer att smälta, på samma sätt som temperaturen i ett glas med isvatten inte stiger över nollpunkten förrän all is har smält. Eftersom egenskaperna för kall och tempererad is är så olika och eftersom de typiskt utgör olika områden i isen så används separata modeller för de två typerna.

Förutom ekvationer som beskriver vad som händer i själva isen krävs även så kallade randvillkor som beskriver vad som händer vid gränsen där isen tar slut.

Isen har olika typer av gränssytor - mot atmosfären ovanför, mot det underliggande berget, mot hav eller land vid iskanten och eventuellt också en gränssyta mellan kall och tempererad is. Alla dessa gränssytor är rörliga och förändras när isens utbredning ändras. Även det underliggande bergets läge ändras eftersom det trycks ner under tyngden av en inlandsis.

De ekvationer som används för den matematiska modellen av inlandsisar kallas Stokes ekvationer och består av balansekvationer och konstituerande ekvationer. Balansekvationerna är generella fysikaliska lagar om massbalans, rörelsemängdens bevarande och energins bevarande som gäller för alla material. De konstituerande ekvationerna beskriver egenskaper som är specifika för isen och omfattar bland annat antagandet att isen är inkompressibel och matematiska samband mellan temperatur och inre energi, viskositet och värmeledningsförmåga.

Trots att Stokes ekvationer är en förenklad beskrivning av verkligheten är de ändå komplicerade och tar så lång tid att lösa att de inte går att använda för en stor is eller långa tidsperioder. I stället kan man använda en förenklad version av Stokes ekvationer som kallas Shallow Ice Approximation (SIA). SIA fungerar för tunna isar, det vill säga isar vars tjocklek är mycket mindre än deras horisontella utbredning. SIA är en matematisk approximation av Stokes ekvationer som är formulerad så att ju mindre kvoten mellan isens tjocklek och dess horisontella utbredning är, desto mer lika blir lösningarna från SIA och Stokes.

I det här projektet har de ekvationer som beskriver temperaturen och isytans förändring i SIA införts i en datormodell som sedan tidigare kunde användas för att beräkna krafter och hastigheter i en kall is med en fast geometri. Den matematiska modellen har diskretiserats och implementerats och sedan har modellen tillämpats på ett enkelt testproblem som även är möjligt att lösa med Stokes fullständiga ekvationer. Genom att jämföra lösningarna från SIA och Stokes ekvationer fås en uppfattning om hur bra approximationen blir för olika parametrar.

Det visade sig att SIA är mycket bra på att beräkna temperaturer och isytans läge medan beräkningarna av ishastigheter som redan fanns implementerade var mer känsliga för att isen verkligen var stor och tunn. Resultaten blev också mycket bättre när en lägre lutning användes, vilket kan hänga samman med att hastigheterna blir lägre och isytans förändring minskar. I det här projektet gjordes inga simuleringar av verkliga isar eftersom SIA-modellen bara är avsedd för vissa enklare regioner i isen. För att simulera en riktig is bör SIA kombineras med mer avancerade modeller i svårare områden. I detta projekt utvärderades endast hur väl SIA approximerar Stokes ekvationer.

# Contents

1	Introduction	7
1.1	The relevance of ice sheet modeling . . . . .	7
1.2	Current state of ice sheet modeling . . . . .	7
1.3	Aim of this work . . . . .	8
2	The Stokes equations	8
2.1	Balance equations . . . . .	8
2.2	Constitutive equations . . . . .	10
2.3	Boundary conditions . . . . .	12
3	Implementation of the energy equation in SIA	13
3.1	Scaling of the energy equation and associated boundary conditions . .	13
3.2	Perturbation expansion . . . . .	15
3.3	Scaling back to dimensional form . . . . .	15
3.4	Sigma transformation . . . . .	16
3.5	Discretization of the temperature equation . . . . .	17
3.5.1	Central and staggered grid . . . . .	17
3.5.2	Preparation of equations for discretization . . . . .	18
3.5.3	Discretization of temperature derivatives . . . . .	18
3.5.4	Discretised equation . . . . .	19
3.6	Resulting formula . . . . .	20
4	Implementation of free surface evolution in SIA	22
4.1	Discretization of the free surface equation . . . . .	22
5	The SIA algorithm	23
5.1	The existing SIA algorithm . . . . .	23
5.2	New algorithm with temperature implemented . . . . .	24
5.3	New algorithm with temperature and free surface evolution imple- mented . . . . .	24
6	Method for comparison with ElmerIce	25
6.1	About ElmerIce . . . . .	25
6.2	Test problem . . . . .	25
6.3	Grid resolution and time step for SIA . . . . .	26
6.4	Grid resolution and time step for ElmerIce . . . . .	26
7	Results	26
7.1	Comparison with ElmerIce with large aspect ratio . . . . .	27
7.2	Comparison with ElmerIce with small aspect ratio . . . . .	27
7.3	Comparison with ElmerIce with large aspect ratio and small slope . .	27
7.4	Temperature and velocity fields in SIA after 10 000 years . . . . .	30
8	Discussion and conclusions	30
	References	31

# 1 Introduction

## 1.1 The relevance of ice sheet modeling

An ice sheet is defined as an ice mass that covers more than 50,000 km<sup>2</sup>. Currently we have two ice sheets on Earth which are located on Antarctica and Greenland. These ice masses constitute an enormous water storage such that if both of them were to melt completely it would cause a sea level rise of almost 70 meters. Historically the extent of ice sheets has varied and it is clear that this plays a role in climate dynamics. Numerical ice sheet modeling is an important tool when it comes to predicting the behavior of ice sheets and their response to and impact on the global climate, [4].

Figure 1 shows the profile of an ice sheet which consists of a cold upper layer and a temperate layer below. The temperate layer is a region where the ice reaches melting temperature due to pressure, friction and geothermal heat. The boundary between the cold and the temperate region is called the cold-temperate-transition surface (CTS). The ice margin can either be on land, as on the left side of the figure, or to the sea, where the ice sheet is connected to a floating ice shelf as on the right side of the figure, [4].

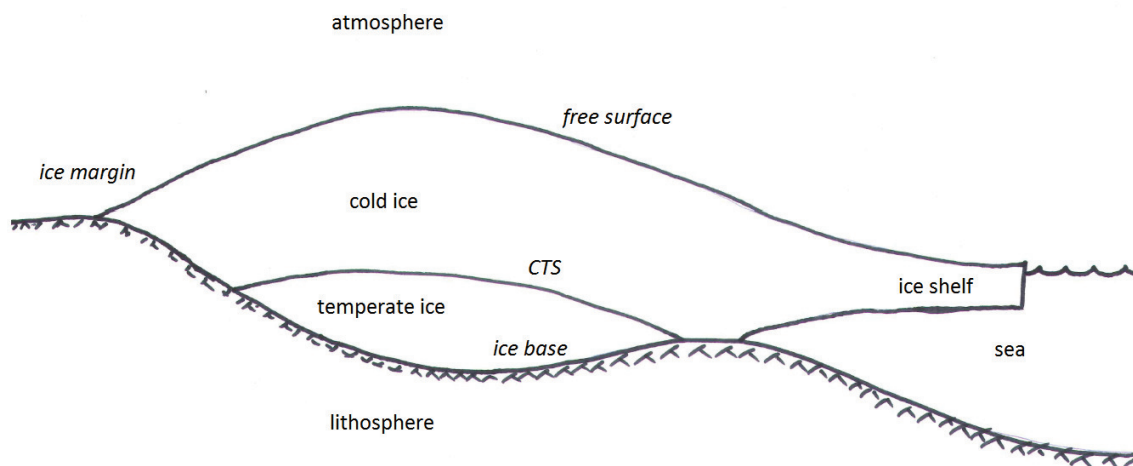


Figure 1: Ice sheet with different kinds of boundaries and regions specified

## 1.2 Current state of ice sheet modeling

Numerical ice modeling is generally based on a mathematical model called the Stokes equations. These provide the most accurate ice model available, but to solve them fully takes a lot of computational power. There is however a numerical solver for the full Stokes equations called "Elmer Ice" which can be used for limited problems, [8].

For large ice sheets and longer time scales, a widely used approximation of the Stokes equations is the Shallow Ice Approximation, SIA. The SIA is a zeroth order perturbation expansion of the Stokes equations which is only valid when the aspect ratio, the vertical extent divided by the horizontal extent of the ice, is very small.

Even for large ice sheets there are regions where SIA fails as higher order dynamics locally play a significant role, e.g. ice streams and ice divides, [4].

Several models have been developed where certain higher order terms have been included. The Second Order Shallow Ice Approximation, SOSIA, is a consistent second order perturbation expansion of the Stokes equations, [1],[3].

### 1.3 Aim of this work

The SIA has been implemented in the ice sheet model SICOPOLIS, written in Fortran 90. In this work we consider an existing implementation of SIA in Matlab which so far computes the stresses, pressures and velocities for steady-state conditions, [1]. Significant simplifications have been made in the Matlab implementation compared to SICOPOLIS - the temperature is held constant, ice thickness does not change over time, the lithosphere is considered rigid, there is no slip between the ice and the underlying bedrock and there is only cold, below-melting-temperature ice. The point of the Matlab implementation is that it can be used for a SOSIA model which first computes a SIA solution and then a SOSIA solution, where the results from the SIA solution are used to compute the SOSIA solution, [1].

The aim of this work is to implement variations in ice temperature over space and time as well as a moving ice surface in the Matlab version of SIA. The result is evaluated by comparison of SIA and full Stokes solutions to a simple test problem. Only the cold ice region is considered.

## 2 The Stokes equations

The mathematical model of glacier dynamics called the Stokes equations is based on the one hand on balance equations, which are general and apply to any material body, and on the other hand on so-called constitutive equations, which are material-specific for ice. Together, they constitute a model that describes the behavior of glacier ice. In the following sections the full Stokes equations are presented according to [4].

### 2.1 Balance equations

There are three balance equations governing the Stokes model. The balance of mass,

$$0 = \dot{\rho} + \rho \nabla \cdot \mathbf{v}, \quad (1)$$

states that the time rate of change of mass in a fixed volume is equal to the net flow of mass across the surface and is called the continuity equation, where  $\rho$  is the mass density and  $\nabla \cdot \mathbf{v}$  is the divergence of the velocity vector field. Superposed dots denotes the material time derivative as defined in [4].

The balance of linear momentum,

$$\rho \dot{\mathbf{v}} = \nabla \cdot \mathbf{T} + \rho \mathbf{g}, \quad (2)$$

states that the time rate of change of linear momentum of a given set of particles is equal to the vector sum of all external forces acting on the particles of the set. The

(effective) gravitational acceleration is denoted  $\mathbf{g}$  and  $\mathbf{T}$  is the Cauchy stress tensor. The Cauchy stress tensor is symmetrical and can be written as

$$\mathbf{T} = \begin{pmatrix} t_{xx} & t_{xy} & t_{xz} \\ t_{xy} & t_{yy} & t_{yz} \\ t_{xz} & t_{yz} & t_{zz} \end{pmatrix}$$

and describes the external forces on a given volume element. The stress vector on a cut along the  $xy$ -plane, perpendicular to  $z$ , is the product of the Cauchy stress tensor and the normal vector in the  $z$ -direction:

$$\begin{pmatrix} t_{xx} & t_{xy} & t_{xz} \\ t_{xy} & t_{yy} & t_{yz} \\ t_{xz} & t_{yz} & t_{zz} \end{pmatrix} \begin{pmatrix} 0 \\ 0 \\ 1 \end{pmatrix} = \begin{pmatrix} t_{xz} \\ t_{yz} \\ t_{zz} \end{pmatrix}.$$

The elements on the diagonal ( $t_{xx}$ ,  $t_{yy}$  and  $t_{zz}$ ) are the normal stresses and the other elements are shear stresses, see Figure 2. The symmetry of the Cauchy stress tensor implies balance of angular momentum.

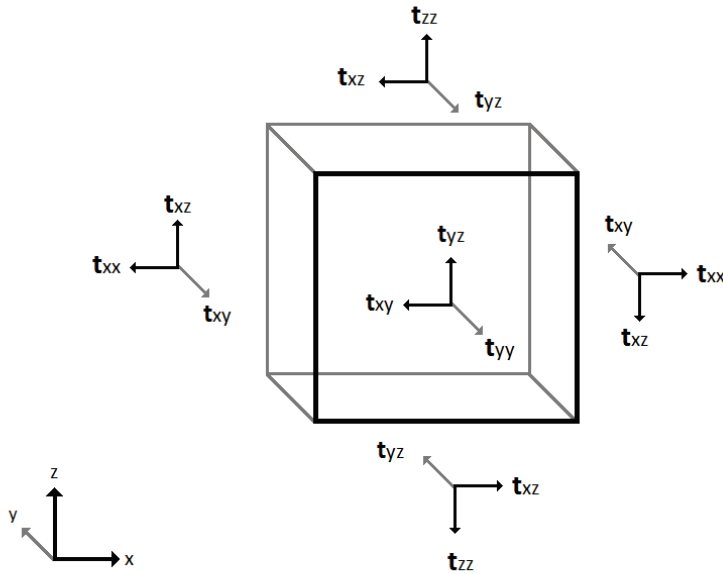


Figure 2: Physical interpretation of the Cauchy tensor components. For simplicity the stress on the furthest surface is omitted.

The balance of internal energy is expressed as

$$\rho \dot{\epsilon} = -\nabla \cdot \mathbf{q} + \mathbf{T} \cdot \mathbf{D} + \rho r, \quad (3)$$

and states that the change of internal energy,  $\rho \dot{\epsilon}$ , depends on convection, dissipation and radiation. The convection term is expressed as the divergence of heat flux  $-\nabla \cdot \mathbf{q}$ , where positive flux is directed away from the point in question. This term includes both advection (heat transfer with bulk motion) and diffusion (conduction). The second term  $\mathbf{T} \cdot \mathbf{D}$  is the dissipation, that is, the heat produced by large scale motion

due to friction.  $\mathbf{D}$  is the strain rate tensor which is also symmetrical and can be written as

$$\mathbf{D} = \begin{pmatrix} D_{xx} & D_{xy} & D_{xz} \\ D_{xy} & D_{yy} & D_{yz} \\ D_{xz} & D_{yz} & D_{zz} \end{pmatrix},$$

where the diagonal elements are dilatation rates

$$D_{xx} = \frac{\partial v_x}{\partial x}, \quad D_{yy} = \frac{\partial v_y}{\partial y}, \quad D_{zz} = \frac{\partial v_z}{\partial z},$$

and the off-diagonal elements are half the shear rates

$$D_{xy} = \frac{1}{2} \left( \frac{\partial v_x}{\partial y} + \frac{\partial v_y}{\partial x} \right), \quad D_{xz} = \frac{1}{2} \left( \frac{\partial v_x}{\partial z} + \frac{\partial v_z}{\partial x} \right), \quad D_{yz} = \frac{1}{2} \left( \frac{\partial v_y}{\partial z} + \frac{\partial v_z}{\partial y} \right).$$

The last term in the balance of internal energy,  $\rho r$ , is the heat supplied by radiation and is neglected in the case of ice sheet modeling as it does not affect ice deeper down than one meter from the free surface, [5].

In the derivation of those equations the Coriolis effect is neglected, as it is comparatively very small, and the centrifugal effect caused by the rotation of the Earth is combined with the gravitational force into effective gravitation. It is also assumed that the ice is a homogeneous one-component material, that is, that the ice is clean. A polar stereographic projection is used which conserves angles but not distances and areas - even for Antarctica this gives a maximum error of 3% on distances, which is considered acceptable. An approximately flat Earth is thus assumed, [4].

## 2.2 Constitutive equations

While the balance equations are general and describe any material body, the constitutive equations describe the material specific behavior. Here we deal with cold ice that is assumed to be incompressible, such that

$$\dot{\rho} = 0 \tag{4}$$

holds, and the mass balance in Equation (1) reduces to

$$\nabla \cdot \mathbf{v} = 0. \tag{5}$$

Under this condition, the Cauchy stress tensor can be rewritten as

$$\mathbf{T} = -p\mathbf{I} + \mathbf{T}^E, \tag{6}$$

where  $p$  is the hydrostatic pressure and  $\mathbf{T}^E$  is called the extra-stress tensor. When this is inserted into the balance of linear momentum, Equation (2), we obtain

$$\rho \dot{\mathbf{v}} = -\nabla p + \nabla \cdot \mathbf{T}^E + \rho \mathbf{g}. \tag{7}$$

Changes in internal energy are related to changes in temperature by

$$\dot{\varepsilon} = c(T)\dot{T}, \tag{8}$$

where  $c(T)$  is the specific heat. As the ice is regarded as incompressible it is not necessary to distinguish between specific heat at constant pressure,  $c_p$ , and specific

Parameter	Value
Stress exponent, $n$	3
Constant, $A_0$	$\left\{ \begin{array}{ll} 3.985 * 10^{-13} \text{ s}^{-1} \text{ Pa}^{-3} & (\text{for } T' \leq 263.15 \text{ K}) \\ 1.916 * 10^3 \text{ s}^{-1} \text{ Pa}^{-3} & (\text{for } T' > 263.15 \text{ K}) \end{array} \right.$
Activation energy, $Q$	$\left\{ \begin{array}{ll} 60 \text{ kJ mol}^{-1} & (\text{for } T' \leq 263.15 \text{ K}) \\ 139 \text{ kJ mol}^{-1} & (\text{for } T' > 263.15 \text{ K}) \end{array} \right.$

Table 1: Stress exponent and parameters for the Arrhenius law, [5].

heat at constant volume,  $c_v$ . The temperature dependency on the other hand is relevant, and is described by the linear equation

$$c(T) = 146.3 + 7.253T \text{ J kg}^{-1} \text{ K}^{-1}, \quad (9)$$

where the temperature is given in Kelvin, [4]. The heat flux  $\mathbf{q}$  is described by Fourier's law

$$\mathbf{q} = -\kappa(T)\nabla T, \quad (10)$$

where  $\kappa$  is the coefficient of heat conductivity

$$\kappa(T) = 9.828e^{-0.0057T} \text{ W m}^{-1} \text{ K}^{-1}. \quad (11)$$

The relation between the extra-stress tensor and the strain rate tensor is described by Glen's flow law

$$\mathbf{D} = EA(T')f(\sigma)\mathbf{T}^E, \quad (12)$$

where  $A$  is the rate factor which is a function of the pressure melting point corrected temperature  $T'$ , and  $f$  is the creep response function with the effective stress  $\sigma$  as argument.  $E$  is the enhancement factor that can be set to a value greater than one to account for softer ice due to impurities. The factor  $EA(T')f(\sigma)$  is related to the viscosity  $\eta$  by

$$\frac{1}{\eta} = 2EA(T')f(\sigma). \quad (13)$$

The rate factor  $A(T')$  can be described by Arrhenius law

$$A(T') = A_0 e^{\frac{-Q}{RT'}}, \quad (14)$$

where

$$T' = T - T_{melt}(p), \quad (15)$$

and values for the constant  $A_0$  and activation energy  $Q$  are presented in Table 1.  $R$  is the universal gas constant. The melting temperature of glacier ice,  $T_{melt}$ , is a linear function of the pressure  $p$

$$T_{melt} = T_0 - \beta p, \quad (16)$$

where  $T_0 = 273.15\text{K}$  and  $\beta$  is the Clausius-Clapeyron constant, which for realistic conditions in air-saturated ice is  $\beta = 9.8 * 10^{-8} \text{ K Pa}^{-1}$ , [4]. The creep response function can be described by the power law

$$f(\sigma) = \sigma^2, \quad (17)$$

where

$$\sigma^2 = \frac{1}{2} \text{tr}(\mathbf{T}^E)^2 = (t_{xz}^E)^2 + (t_{yz}^E)^2 + (t_{xy}^E)^2 + \frac{1}{2} \left( (t_{xx}^E)^2 + (t_{yy}^E)^2 + (t_{zz}^E)^2 \right) \quad (18)$$

Glens' flow law, Equation (12), can give rise to an infinitely large viscosity as the creep function is zero for zero effective stress. This is not physically problematic as the strain rate will be very small for small stresses, but in the mathematical solution this may introduce a singularity in the equations for the velocity field. Several modified flow laws exist for this reason. One alternative is to add a small constant,  $\sigma_{res}$ , to  $\sigma$  in order to prevent it from ever becoming zero, another is to put a lower bound on the  $\sigma$ -value, [4].

When we insert the constitutive Equations (6), (8), (10) and (12) into the energy balance, Equation (3), and neglect the radiation term we obtain

$$\rho c(T) \dot{T} = \nabla \cdot \kappa(T) \nabla T + (-p\mathbf{I} + \mathbf{T}^E) \cdot (EA(T') f(\sigma) \mathbf{T}^E), \quad (19)$$

which can be rewritten as in [1]:

$$\rho c(T) \left( \frac{\partial T}{\partial t} + (\nabla T) \mathbf{v} \right) = \nabla \cdot \kappa(T) \nabla T + 2EA(T') f(\sigma) \sigma^2. \quad (20)$$

## 2.3 Boundary conditions

At the free surface the stress of the atmospheric pressure,  $p_{atm}$ , and wind shear,  $\tau_{wind}$ , are neglected so that

$$\mathbf{T}_{ice} \mathbf{n} = \mathbf{T}_{atm} \mathbf{n} = -p_{atm} \mathbf{n} + \boldsymbol{\tau}_{wind} \approx 0, \quad (21)$$

where  $\mathbf{n}$  is the normal vector to the free surface. The kinematic condition at the free surface is

$$\frac{\partial h}{\partial t} + \frac{\partial h}{\partial x} v_x + \frac{\partial h}{\partial y} v_y - v_z = \sqrt{1 + \frac{\partial h^2}{\partial x^2} + \frac{\partial h^2}{\partial y^2}} a^\perp \quad (22)$$

where  $h$  is the position of the ice surface and  $a^\perp$  is the accumulation-ablation function, that is, the volume flow per unit area perpendicular to the free surface, [3],[4]. The factor  $\sqrt{1 + \frac{\partial h^2}{\partial x^2} + \frac{\partial h^2}{\partial y^2}}$  accounts for the difference between the perpendicular flux  $a^\perp$  and the vertical flux  $a$ . At the base, a no-slip condition is applied and the lithosphere is considered as rigid.

The ice temperature at the surface is set to equal the temperature of the atmosphere

$$T_{ice} = T_{atm}, \quad (23)$$

and the boundary condition for the temperature at the base becomes

$$\kappa_i(T_i) (\nabla T_i \cdot \mathbf{n}) - \kappa_r(T_r) (\nabla T_r \cdot \mathbf{n}) = 0, \quad (24)$$

as is shown in [3]. The subscript  $r$  denotes properties of the lithosphere, and  $i$  ice properties.

### 3 Implementation of the energy equation in SIA

As mentioned earlier, the Shallow Ice Approximation (SIA) is a much used approximation for the Stokes equations when it comes to ice sheet modeling. In order to derive the SIA equations the Stokes equations are scaled into a non-dimensional form, using typical values for the different parameters in order to determine which components are of significance for the solution and which ones can be neglected. The aspect ratio,

$$\epsilon = \frac{[H]}{[L]}, \quad (25)$$

is then used in a perturbation expansion.  $[H]$  is the typical vertical extent of the ice sheet and  $[L]$  is the typical horizontal extent. As the SIA is a zeroth order approximation, all terms containing  $\epsilon$  are neglected. The square brackets denote a typical values. Figure 3 shows the notations used for boundaries, horizontal extent and ice thickness. As this work is focused on implementing temperature variations in SIA, the derivation of SIA will be demonstrated on the energy balance and its boundary conditions.

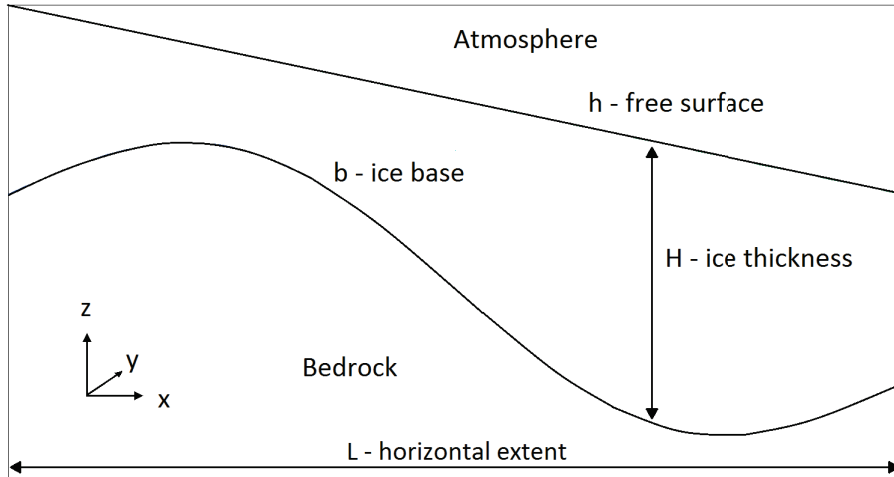


Figure 3: Notations for boundaries, horizontal extent and ice thickness

#### 3.1 Scaling of the energy equation and associated boundary conditions

The following scaling of the energy balance equation is done as by Baral et al. in [3], where the procedure is done for the entire set of equations. The energy equation as expressed in Equation (20) is rewritten in component form for a Cartesian coordinate system with  $x$  and  $y$  as horizontal coordinates and  $z$  as the vertical coordinate,

$$\begin{aligned} \rho c(T) \left( \frac{\partial T}{\partial t} + v_x \frac{\partial T}{\partial x} + v_y \frac{\partial T}{\partial y} + v_z \frac{\partial T}{\partial z} \right) = \\ = \frac{\partial}{\partial x} \left( \kappa(T) \frac{\partial T}{\partial x} \right) + \frac{\partial}{\partial y} \left( \kappa(T) \frac{\partial T}{\partial y} \right) + \frac{\partial}{\partial z} \left( \kappa(T) \frac{\partial T}{\partial z} \right) + 2EA(T')f(\sigma)\sigma^2. \end{aligned} \quad (26)$$

$(x, y)$	$=$	$[L](\tilde{x}, \tilde{y})$
$(z, b)$	$=$	$[H](\tilde{z}, \tilde{b})$
$(v_x, v_y)$	$=$	$[V_L](\tilde{v}_x, \tilde{v}_y)$
$v_z$	$=$	$[V_H]\tilde{v}_z$
$t$	$=$	$([L]/[V_L])\tilde{t}$
$(T, T')$	$=$	$[\Delta T](\tilde{\Theta}, \tilde{\Theta}')$
$A(T')$	$=$	$[A]\tilde{A}(\tilde{\Theta}')$
$\sigma$	$=$	$\epsilon \rho g [H] \tilde{\sigma}$
$f(\sigma)$	$=$	$[f]\tilde{f}(\tilde{\sigma})$
$\kappa(T)$	$=$	$[\kappa]\tilde{\kappa}(\tilde{\Theta})$
$\kappa_r$	$=$	$[\kappa_r]\tilde{\kappa}_r$
$c(T)$	$=$	$[c]\tilde{c}(\tilde{\Theta})$

Table 2: Scaling of parameters

and the boundary condition in Equation (24) in component form becomes

$$\kappa_i(T_i) \left( \frac{\partial T_i}{\partial x} \frac{\partial b}{\partial x} + \frac{\partial T_i}{\partial y} \frac{\partial b}{\partial y} - \frac{\partial T_i}{\partial z} \right) - \kappa_r \left( \frac{\partial T_r}{\partial x} \frac{\partial b}{\partial x} + \frac{\partial T_r}{\partial y} \frac{\partial b}{\partial y} - \frac{\partial T_r}{\partial z} \right) = 0. \quad (27)$$

A scaling is then done as in [3] by transforming the parameters according to Table 2. Dimensionless products are also introduced in the scaling,

$$\begin{aligned} \epsilon &= \frac{[H]}{[L]}, \\ \mathcal{D} &= \frac{[\kappa]}{\rho [c] [H] [V_H]}, \\ \alpha &= \frac{g [H]}{[c] [\partial T]}, \\ \mathcal{K} &= \frac{\rho g [H]^3 [A] [f]}{[L] [V_L]}, \end{aligned} \quad (28)$$

out of which  $\epsilon$  is several orders of magnitude smaller than the others, [3]. When Equation (26) is scaled as in Table 2 and the dimensionless products are inserted, we obtain

$$\begin{aligned} &\tilde{c}(\tilde{\Theta}) \left( \frac{\partial \tilde{\Theta}}{\partial \tilde{t}} + \tilde{v}_x \frac{\partial \tilde{\Theta}}{\partial \tilde{x}} + \tilde{v}_y \frac{\partial \tilde{\Theta}}{\partial \tilde{y}} + \tilde{v}_z \frac{\partial \tilde{\Theta}}{\partial \tilde{z}} \right) = \\ &= \mathcal{D} \left( \epsilon^2 \frac{\partial}{\partial \tilde{x}} (\tilde{\kappa}(\tilde{\Theta}) \frac{\partial \tilde{\Theta}}{\partial \tilde{x}}) + \epsilon^2 \frac{\partial}{\partial \tilde{y}} (\tilde{\kappa}(\tilde{\Theta}) \frac{\partial \tilde{\Theta}}{\partial \tilde{y}}) + \frac{\partial}{\partial \tilde{z}} (\tilde{\kappa}(\tilde{\Theta}) \frac{\partial \tilde{\Theta}}{\partial \tilde{z}}) \right) + 2\alpha \mathcal{K} E \tilde{A}(\tilde{\Theta}') \tilde{f}(\tilde{\sigma}) \tilde{\sigma}^2, \end{aligned} \quad (29)$$

while the boundary condition for the temperature at the cold ice base in Equation (24), [3], becomes

$$\tilde{\kappa}(\tilde{\Theta}) \left( \epsilon^2 \frac{\partial \tilde{\Theta}}{\partial \tilde{x}} \frac{\partial \tilde{b}}{\partial \tilde{x}} + \epsilon^2 \frac{\partial \tilde{\Theta}}{\partial \tilde{y}} \frac{\partial \tilde{b}}{\partial \tilde{y}} - \frac{\partial \tilde{\Theta}}{\partial \tilde{z}} \right) - \frac{[\kappa_r]}{[\kappa]} \tilde{\kappa}_r \left( \epsilon^2 \frac{\partial \tilde{\Theta}_r}{\partial \tilde{x}} \frac{\partial \tilde{b}}{\partial \tilde{x}} + \epsilon^2 \frac{\partial \tilde{\Theta}_r}{\partial \tilde{y}} \frac{\partial \tilde{b}}{\partial \tilde{y}} - \frac{\partial \tilde{\Theta}_r}{\partial \tilde{z}} \right) = 0. \quad (30)$$

### 3.2 Perturbation expansion

To obtain the SIA version of the energy equation a perturbation expansion is introduced where all variables are expressed as a power series of  $\epsilon$ . The tilde signs are omitted for simplicity:

$$\begin{aligned}\Theta &= \sum_{i=0}^{\infty} \epsilon^i \Theta_{(i)} = \epsilon^0 \Theta_{(0)} + \epsilon^1 \Theta_{(1)} + \epsilon^2 \Theta_{(2)} + \dots \\ v &= \sum_{i=0}^{\infty} \epsilon^i v_{(i)} = \epsilon^0 v_{(0)} + \epsilon^1 v_{(1)} + \epsilon^2 v_{(2)} + \dots \\ \sigma &= \sum_{i=0}^{\infty} \epsilon^i \sigma_{(i)} = \epsilon^0 \sigma_{(0)} + \epsilon^1 \sigma_{(1)} + \epsilon^2 \sigma_{(2)} + \dots\end{aligned}\quad (31)$$

These are inserted into Equation (29), and then all terms of the zeroth order are equated. This corresponds to neglecting the horizontal heat conduction in the energy equation

$$\begin{aligned}c(\Theta_{(0)}) \left( \frac{\partial \Theta_{(0)}}{\partial t} + v_{x(0)} \frac{\partial \Theta_{(0)}}{\partial x} + v_{y(0)} \frac{\partial \Theta_{(0)}}{\partial y} + v_{z(0)} \frac{\partial \Theta_{(0)}}{\partial z} \right) = \\ = \mathcal{D} \frac{\partial}{\partial z} \left( \kappa(\Theta_{(0)}) \frac{\partial \Theta_{(0)}}{\partial z} \right) + 2\alpha \mathcal{K} E A(\Theta'_{(0)}) f(\sigma_{(0)}) (\sigma_{(0)})^2.\end{aligned}\quad (32)$$

In the expression for  $\sigma$  the horizontal plane shear stress and normal stresses are neglected in the zeroth order approximation, which is not shown here but also affects the temperature.

The SIA boundary condition at the base becomes

$$-\kappa(\Theta_{(0)}) \frac{\partial \Theta_{(0)}}{\partial z} + \frac{[\kappa_r]}{[\kappa]} \kappa_r(\Theta_{r(0)}) \frac{\partial \Theta_{r(0)}}{\partial z} = 0.\quad (33)$$

### 3.3 Scaling back to dimensional form

In the code SIA is implemented in dimensional form, so we scale back Equation (32) and get

$$\rho c(T) \left( \frac{\partial T}{\partial t} + v_x \frac{\partial T}{\partial x} + v_y \frac{\partial T}{\partial y} + v_z \frac{\partial T}{\partial z} \right) = \frac{\partial}{\partial z} \left( \kappa(T) \frac{\partial T}{\partial z} \right) + 2EA(T') f(\sigma) \sigma^2.\quad (34)$$

The boundary condition at the cold ice base, Equation (33) becomes

$$-\kappa \frac{\partial T}{\partial z} + \kappa_r \frac{\partial T_r}{\partial z} = 0,\quad (35)$$

which can also be expressed as

$$\kappa \frac{\partial T}{\partial z} = -q_{geo}^\perp,\quad (36)$$

where  $q_{geo}^\perp$  is the geothermal heat flux, typically around 50 mW/m<sup>2</sup>, [6]. The boundary condition at the free surface remains unchanged in SIA as

$$T_{ice} = T_{atm}.\quad (37)$$

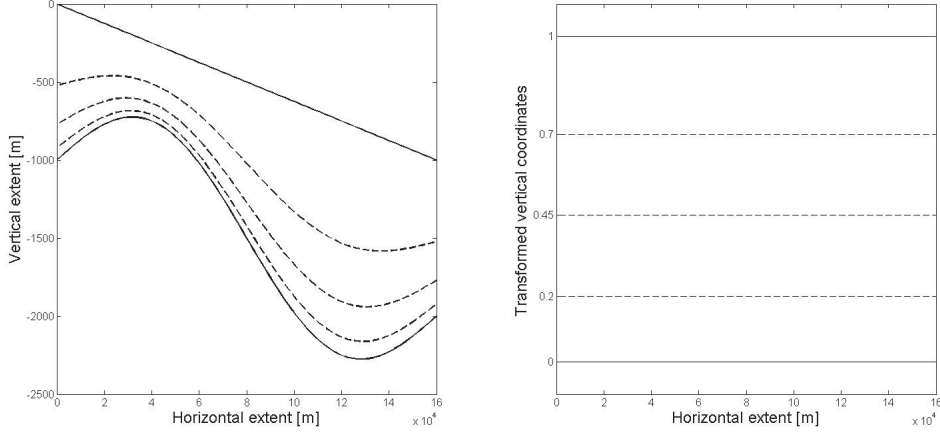


Figure 4: A cut through the ice showing the vertical shape of the transformed grid

### 3.4 Sigma transformation

The use of a regular, rectangular grid with constant spacings in the discretization would cause the boundaries - the free surface and the ice base - to generally fall between grid points. This would make the computations complicated and introduces new inaccuracies when values have to be interpolated. To avoid that, a so-called  $\sigma$ -transformation is done, where the vertical coordinate is mapped onto the interval  $[0,1]$ , see Figure 4.

The horizontal coordinates are not affected by the transformation, so the margins of the ice can still fall between grid points when the model is applied to a real ice sheet. At the margins another problem also occurs because of the  $\sigma$ -transformation when an ice thickness of zero is mapped onto the unity interval. This introduces a singularity that has to be dealt with in some way, [4]. However, such problems do not occur in the test problem used in this report and will not be considered here.

The following coordinate transformation is done for the cold ice region, as by Ahlkrona in [1]:

$$\begin{aligned}
 x &= \xi \\
 y &= \eta \\
 \frac{z - b}{H} &= \frac{e^{a\zeta} - 1}{e^a - 1} =: \varepsilon(\zeta) \\
 t &= \tau
 \end{aligned} \tag{38}$$

where  $a$  is a stretching parameter which is normally 2. When transforming equations, all derivatives are affected, not only the vertical derivatives. With the abbreviation

$$(m, \mu) \in \{(x, \xi), (y, \eta), (t, \tau)\}$$

the transformation of horizontal derivatives and time derivatives for cold ice becomes

$$\frac{\partial}{\partial m} = \frac{\partial}{\partial \mu} - \frac{1}{Hae^{a\zeta}} \left( (e^a - 1) \frac{\partial b}{\partial \mu} + (e^{a\zeta} - 1) \frac{\partial H}{\partial \mu} \right) \frac{\partial}{\partial \zeta} \tag{39}$$

and for vertical derivatives we obtain

$$\frac{\partial}{\partial z} = \frac{e^a - 1}{Hae^{a\zeta}} \frac{\partial}{\partial \zeta}. \tag{40}$$

The energy equation after sigma transformation becomes

$$\begin{aligned}
& \rho c(T) \left( \frac{\partial T}{\partial \tau} - \frac{1}{Hae^{a\zeta}} \left( (e^a - 1) \frac{\partial b}{\partial \tau} + (e^{a\zeta} - 1) \frac{\partial H}{\partial \tau} \right) \frac{\partial T}{\partial \zeta} \right. \\
& + v_x \left( \frac{\partial T}{\partial \xi} - \frac{1}{Hae^{a\zeta}} \left( (e^a - 1) \frac{\partial b}{\partial \xi} + (e^{a\zeta} - 1) \frac{\partial H}{\partial \xi} \right) \frac{\partial T}{\partial \zeta} \right) \\
& + v_y \left( \frac{\partial T}{\partial \eta} - \frac{1}{Hae^{a\zeta}} \left( (e^a - 1) \frac{\partial b}{\partial \eta} + (e^{a\zeta} - 1) \frac{\partial H}{\partial \eta} \right) \frac{\partial T}{\partial \zeta} \right) \\
& \left. + v_z \frac{e^a - 1}{Hae^{a\zeta}} \frac{\partial T}{\partial \zeta} \right) \\
& = \frac{e^a - 1}{Hae^{a\zeta}} \frac{\partial}{\partial \zeta} \left( \kappa(T) \frac{e^a - 1}{Hae^{a\zeta}} \frac{\partial T}{\partial \zeta} \right) + 2EA(T') f(\sigma) \sigma^2.
\end{aligned} \tag{41}$$

The boundary condition at the surface remains unchanged. The condition for the base, Equation (36), becomes after sigma transformation

$$\kappa \frac{e^a - 1}{Hae^{a\zeta}} \frac{\partial T}{\partial \zeta} = -q_{geo}^\perp. \tag{42}$$

## 3.5 Discretization of the temperature equation

### 3.5.1 Central and staggered grid

For stability reasons, double grids are used in each direction - one primary or *main* grid, and one secondary or *staggered* grid. The staggered grid is shifted half a grid step, so that the point  $i_s = 1$  on the staggered grid is located in the middle between  $i_m = 1$  and  $i_m = 2$  on the main grid, see figure 5. Velocities and stresses are defined on the staggered grid and all other parameters on the main grid. When a variable is needed in a point where it is not defined, the arithmetic mean value of the adjacent values is used.

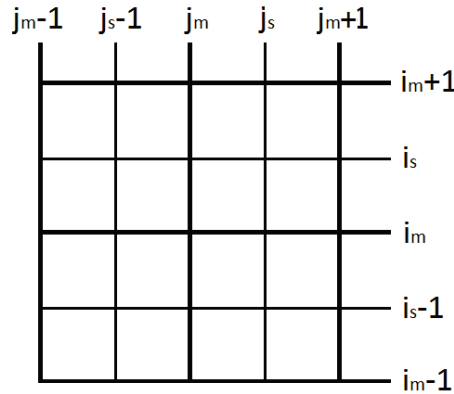


Figure 5: Illustration of how the main grid and the staggered grid overlap. For simplicity the figure shows a 2D grid.

The main grid is indexed  $i_m=1,\dots,IMAX+1$  in  $\xi$ -direction,  $j_m=1,\dots,JMAX+1$  in  $\eta$ -direction and  $k_m=1,\dots,KMAX+1$  in  $\zeta$ -direction. In the  $\zeta$ -direction (vertical),

$k_m=1$  corresponds to the ice base and  $k_m=KMAX+1$  to the ice surface. The staggered grid has corresponding indexing  $i_s, j_s$  and  $k_s$  but with one grid point less in each direction.

### 3.5.2 Preparation of equations for discretization

Before starting the discretization we neglect  $\frac{\partial b}{\partial \tau}$  as we are going to assume a stiff lithosphere and thus Equation (41) simplifies to

$$\begin{aligned} & \frac{\partial T}{\partial \tau} + v_x \frac{\partial T}{\partial \xi} + v_y \frac{\partial T}{\partial \eta} \\ & + \left( v_z \frac{e^a - 1}{Hae^{a\zeta}} - v_x \left( \frac{e^a - 1}{Hae^{a\zeta}} \frac{\partial b}{\partial \xi} + \frac{e^a - 1}{Hae^{a\zeta}} \frac{\partial H}{\partial \xi} \right) \right. \\ & \quad \left. - v_y \left( \frac{e^a - 1}{Hae^{a\zeta}} \frac{\partial b}{\partial \eta} + \frac{e^a - 1}{Hae^{a\zeta}} \frac{\partial H}{\partial \eta} \right) - \frac{1}{Hae^{a\zeta}} (e^{a\zeta} - 1) \frac{\partial H}{\partial \tau} \right) \frac{\partial T}{\partial \zeta} \\ & = \frac{1}{\rho c(T)} \frac{e^a - 1}{Hae^{a\zeta}} \frac{\partial}{\partial \zeta} \left( \kappa(T) \frac{e^a - 1}{Hae^{a\zeta}} \frac{\partial T}{\partial \zeta} \right) + \frac{2EA(T')}{\rho c(T)} f(\sigma) \sigma^2. \end{aligned} \quad (43)$$

Set vertical advection

$$\begin{aligned} W & = v_z \frac{e^a - 1}{Hae^{a\zeta}} - v_x \left( \frac{e^a - 1}{Hae^{a\zeta}} \frac{\partial b}{\partial \xi} + \frac{e^a - 1}{Hae^{a\zeta}} \frac{\partial H}{\partial \xi} \right) \\ & \quad - v_y \left( \frac{e^a - 1}{Hae^{a\zeta}} \frac{\partial b}{\partial \eta} + \frac{e^a - 1}{Hae^{a\zeta}} \frac{\partial H}{\partial \eta} \right) - \frac{1}{Hae^{a\zeta}} (e^{a\zeta} - 1) \frac{\partial H}{\partial \tau} \end{aligned} \quad (44)$$

and we obtain

$$\frac{\partial T}{\partial \tau} + v_x \frac{\partial T}{\partial \xi} + v_y \frac{\partial T}{\partial \eta} + W \frac{\partial T}{\partial \zeta} = \frac{1}{\rho c(T)} \frac{e^a - 1}{Hae^{a\zeta}} \frac{\partial}{\partial \zeta} \left( \kappa(T) \frac{e^a - 1}{Hae^{a\zeta}} \frac{\partial T}{\partial \zeta} \right) + \frac{2EA(T')}{\rho c(T)} f(\sigma) \sigma^2. \quad (45)$$

### 3.5.3 Discretization of temperature derivatives

The discretization of derivatives is done in different ways depending on the nature of the derivative. The time derivative is approximated by a one sided difference

$$\frac{\partial T}{\partial \tau} \sim \frac{T(\tau) - T(\tau - \Delta\tau)}{\Delta\tau}, \quad (46)$$

which is intuitive as the temperature development can only depend on historical and not on future temperatures. The advection terms are discretized using an asymmetric "upstream" scheme, described by

$$\begin{aligned} v_x \frac{\partial T}{\partial \xi} & \sim \begin{cases} v_x(i_s - 1) \frac{T(i_m) - T(i_m - 1)}{\Delta\xi} & \text{if } v_x(i_m) > 0 \\ v_x(i_s) \frac{T(i_m + 1) - T(i_m)}{\Delta\xi} & \text{if } v_x(i_m) < 0 \end{cases} \\ v_y \frac{\partial T}{\partial \eta} & \sim \begin{cases} v_y(j_s - 1) \frac{T(j_m) - T(j_m - 1)}{\Delta\eta} & \text{if } v_y(j_m) > 0 \\ v_y(j_s) \frac{T(j_m + 1) - T(j_m)}{\Delta\eta} & \text{if } v_y(j_m) < 0 \end{cases} \\ W \frac{\partial T}{\partial \zeta} & \sim \begin{cases} W(k_s - 1) \frac{T(k_m) - T(k_m - 1)}{\Delta\zeta} & \text{if } W(k_m) > 0 \\ W(k_s) \frac{T(k_m + 1) - T(k_m)}{\Delta\zeta} & \text{if } W(k_m) < 0 \end{cases} \end{aligned} \quad (47)$$

which is logical considering that the process of advection will transport heat in the flow direction only. This discretization is done according to [4] in a way that differs slightly from how the implementation is done in SICOPOLIS. In SICOPOLIS the condition on the horizontal velocity and vertical advection direction is taken on the staggered grid points, i.e.  $i_s - 1$  and  $i_s$  instead of  $i_m$ .

For the diffusion term a central difference is applied,

$$\frac{\partial}{\partial \zeta} \left( \kappa \frac{e^a - 1}{Hae^{a\zeta}} \frac{\partial T}{\partial \zeta} \right) \sim \frac{1}{\Delta \zeta} \left( \bar{\kappa}(k_s) \frac{e^a - 1}{Hae^{a\zeta(k_s)}} \frac{T(k_m + 1) - T(k_m)}{\Delta \zeta} - \bar{\kappa}(k_s - 1) \frac{e^a - 1}{Hae^{a\zeta(k_s-1)}} \frac{T(k_m) - T(k_m - 1)}{\Delta \zeta} \right), \quad (48)$$

as diffusion is a process that operates in all directions simultaneously.

### 3.5.4 Discretised equation

The temperature equation, Equation (45), is discretized as in Section 3.5.3. The values for the parameters  $c(T)$ ,  $\kappa(T)$ , and  $A(T')$  are all taken from the previous time step as they are functions of the temperature which is not yet computed for the current step. For the horizontal advection terms temperatures from the previous time step are also used as the new values are only available for some directions, that is, for lower indices of  $i$  and  $j$ .

We then obtain

$$\begin{aligned}
& \frac{T(i_m, j_m, k_m, \tau) - T(i_m, j_m, k_m, \tau - 1)}{\Delta\tau} \\
& + \left( v_x(i_s - 1, j_m, k_m, \tau) \frac{T(i_m, j_m, k_m, \tau - 1) - T(i_m - 1, j_m, k_m, \tau - 1)}{\Delta\xi} \right) \quad \text{if } v_x(i_m, j_m, k_m, \tau) > 0 \\
& + \left( v_x(i_s, j_m, k_m, \tau) \frac{T(i_m + 1, j_m, k_m, \tau - 1) - T(i_m, j_m, k_m, \tau - 1)}{\Delta\xi} \right) \quad \text{if } v_x(i_m, j_m, k_m, \tau) < 0 \\
& + \left( v_y(i_m, j_s - 1, k_m, \tau) \frac{T(i_m, j_m, k_m, \tau - 1) - T(i_m, j_m - 1, k_m, \tau - 1)}{\Delta\eta} \right) \quad \text{if } v_y(i_m, j_m, k_m, \tau) > 0 \\
& + \left( v_y(i_m, j_s, k_m, \tau) \frac{T(i_m, j_m + 1, k_m, \tau - 1) - T(i_m, j_m, k_m, \tau - 1)}{\Delta\eta} \right) \quad \text{if } v_y(i_m, j_m, k_m, \tau) < 0 \\
& + W(i_m, j_m, k_s - 1, \tau) \frac{T(i_m, j_m, k_m, \tau) - T(i_m, j_m, k_m - 1, \tau)}{\Delta\zeta} \quad \text{if } W(i_m, j_m, k_m, \tau) > 0 \\
& + W(i_m, j_m, k_s, \tau) \frac{T(i_m, j_m, k_m + 1, \tau) - T(i_m, j_m, k_m, \tau)}{\Delta\zeta} \quad \text{if } W(i_m, j_m, k_m, \tau) < 0 \\
& = \\
& \frac{1}{\rho c(i_m, j_m, k_m, \tau - 1)} \frac{e^a - 1}{H(i_m, j_m) a e^{a\zeta(k_m)}} \frac{1}{\Delta\zeta} \\
& \left( \bar{\kappa}(i_m, j_m, k_s, \tau - 1) \frac{e^a - 1}{H(i_m, j_m) a e^{a\zeta(k_s)}} \frac{T(i_m, j_m, k_m + 1, \tau) - T(i_m, j_m, k_m, \tau)}{\Delta\zeta} \right. \\
& \left. - \bar{\kappa}(i_m, j_m, k_s - 1, \tau - 1) \frac{e^a - 1}{H(i_m, j_m) a e^{a\zeta(k_s - 1)}} \frac{T(i_m, j_m, k_m, \tau) - T(i_m, j_m, k_m - 1, \tau)}{\Delta\zeta} \right) \\
& + \frac{2EA(i_m, j_m, k_m, \tau - 1)}{\rho c(i_m, j_m, k_m, \tau - 1)} f(\sigma(i_m, j_m, k_m, \tau)) \sigma(i_m, j_m, k_m, \tau)^2.
\end{aligned} \tag{49}$$

The boundary condition at the ice base ( $k_m = 1$ ) becomes

$$\kappa(i_m, j_m, k_m, \tau - 1) \frac{e^a - 1}{H(i_m, j_m) a e^{a\zeta(k_m)}} \frac{T(i_m, j_m, k_m + 1, \tau) - T(i_m, j_m, k_m, \tau)}{\Delta\zeta} = -q_{geo}^\perp \tag{50}$$

and at the surface ( $k_m = \text{KMAX} + 1$ )

$$T(i_m, j_m, k_m, \tau) = T_{surf}. \tag{51}$$

### 3.6 Resulting formula

In the Matlab code Equations (49),(50) and (51) are expressed as a tridiagonal system of linear equations for each vertical ice column corresponding to an  $(i, j)$  combination. In the following we do not write all indices explicitly, only those that differ from the current grid point and time, so that if nothing else is stated a parameter is taken at  $(i_m, j_m, k_m, \tau)$ . If Equation (49) is rewritten on the form

$$a * T(k_m - 1) + b * T + c * T(k_m + 1) = d,$$

then the resulting system of linear equations becomes

$$\begin{pmatrix} b_1 & c_1 & 0 & 0 & \cdot & 0 \\ a_2 & b_2 & c_2 & 0 & \cdot & 0 \\ 0 & a_3 & b_3 & c_3 & \cdot & 0 \\ 0 & 0 & a_4 & b_4 & \cdot & 0 \\ \cdot & \cdot & \cdot & \cdot & \cdot & c_{kmax} \\ 0 & 0 & 0 & 0 & a_{kmax} & b_{kmax+1} \end{pmatrix} \begin{pmatrix} T_1 \\ T_2 \\ T_3 \\ T_4 \\ \cdot \\ T_{kmax+1} \end{pmatrix} = \begin{pmatrix} d_1 \\ d_2 \\ d_3 \\ d_4 \\ \cdot \\ d_{kmax+1} \end{pmatrix}$$

which is solved for each combination  $(i, j)$ . Keep in mind that the lowest index denotes the bottom of the ice, so that  $T_1$  is at the base and  $T_{kmax+1}$  is at the free surface. The coefficients  $a(k), b(k), c(k)$  and  $d(k)$  become

$$\begin{aligned} a(k) &= -\frac{1}{\rho c(\tau-1)} \frac{e^a-1}{Hae^{a\zeta}} \frac{\partial \tau}{\partial \zeta^2} \bar{\kappa}(k_s-1) \frac{e^a-1}{Hae^{a\zeta(k_s-1)}} \\ &\quad -W(k_s-1) \frac{\partial \tau}{\partial \zeta} && \text{if } W(k_m) > 0 \\ &\quad +0 && \text{if } W(k_m) \leq 0 \\ \\ b(k) &= 1 + 2 \frac{1}{\rho c(\tau-1)} \left( \frac{e^a-1}{Hae^{a\zeta}} \right)^2 \frac{\partial \tau}{\partial \zeta^2} \bar{\kappa}(\tau-1) \\ &\quad +W(k_s-1) \frac{\partial \tau}{\partial \zeta} && \text{if } W(k_m) > 0 \\ &\quad -W(k_s) \frac{\partial \tau}{\partial \zeta} && \text{if } W(k_m) \leq 0 \\ \\ c(k) &= -\frac{1}{\rho c(\tau-1)} \frac{e^a-1}{Hae^{a\zeta}} \frac{\partial \tau}{\partial \zeta^2} \bar{\kappa}(k_s, \tau-1) \frac{e^a-1}{Hae^{a\zeta(k_s)}} && (52) \\ &\quad +W(k_s) \frac{\partial \tau}{\partial \zeta} && \text{if } W(k_m) < 0 \\ &\quad +0 && \text{if } W(k_m) \leq 0 \\ \\ d(k) &= T(\tau-1) + \frac{2EA(\tau-1)\partial \tau}{\rho c(\tau-1)} f(\sigma)\sigma^2 \\ &\quad -v_x(i_s-1) \frac{T(\tau-1)-T(i_m-1)}{\partial \xi} \partial \tau && \text{if } v_x(i_m) > 0 \\ &\quad -v_x(i_s) \frac{T(i_m+1, \tau-1)-T(\tau-1)}{\partial \xi} \partial \tau && \text{if } v_x(i_m) \leq 0 \\ &\quad -v_y(j_s-1) \frac{T(\tau-1)-T(j_m-1)}{\partial \eta} \partial \tau && \text{if } v_y(j_m) > 0 \\ &\quad -v_y(j_s) \frac{T(j_m+1, \tau-1)-T(\tau-1)}{\partial \eta} \partial \tau && \text{if } v_y(j_m) \leq 0 \end{aligned}$$

where

$$\begin{aligned} W(k) &= v_z \frac{e^a-1}{Hae^{a\zeta}} - v_x \left( \frac{e^a-1}{Hae^{a\zeta}} \frac{\partial b}{\partial \xi} + \frac{e^{a\zeta}-1}{Hae^{a\zeta}} \frac{\partial H}{\partial \xi} \right) - \\ &\quad v_y \left( \frac{e^a-1}{Hae^{a\zeta}} \frac{\partial b}{\partial \eta} + \frac{e^{a\zeta}-1}{Hae^{a\zeta}} \frac{\partial H}{\partial \eta} \right) - \frac{e^{a\zeta}-1}{Hae^{a\zeta}} \frac{\partial H}{\partial \tau}. \end{aligned} \tag{53}$$

The boundary conditions in Equation (51) and (50) provide

$$\begin{aligned}
b(1) &= -\frac{\kappa(k_m = 1)}{\partial\zeta} \frac{e^a - 1}{Ha e^{a\zeta(k_m=1)}} \\
c(1) &= \frac{\kappa(k_m = 1)}{\partial\zeta} \frac{e^a - 1}{Ha e^{a\zeta(k_m=1)}} \\
d(1) &= -q_{geo}^\perp \\
a(kmax + 1) &= 0 \\
b(kmax + 1) &= 1 \\
d(kmax + 1) &= T_{surf}.
\end{aligned} \tag{54}$$

## 4 Implementation of free surface evolution in SIA

The kinematic boundary condition at the free surface, Equation (22), becomes in its SIA version

$$\frac{\partial h}{\partial t} + \frac{\partial h}{\partial x} v_x + \frac{\partial h}{\partial y} v_y - v_z = a^\perp \tag{55}$$

as is shown in [3], and remains the same when scaled back to dimensional form as terms with  $[L]$ ,  $[H]$ ,  $[V_L]$  and  $[V_H]$  cancel each other out. After sigma transformation according to Equation (39) we obtain

$$\frac{\partial h}{\partial \tau} + v_x \frac{\partial h}{\partial \xi} + v_y \frac{\partial h}{\partial \eta} - v_z = a^\perp. \tag{56}$$

The simplicity of the transformed free surface boundary condition is due to the fact that  $\frac{\partial h}{\partial \zeta} = 0$  as the surface has no extent in vertical direction.

### 4.1 Discretization of the free surface equation

As in the temperature equation, the time derivative is discretized using a simple backward difference, Equation (46), while the asymmetric upstream scheme in Equation (47) is applied to the spatial derivatives. The discretized free surface equation becomes

$$\begin{aligned}
&\frac{h(i_m, j_m, \tau) - h(i_m, j_m, \tau - \Delta\tau)}{\Delta\tau} \\
&+ v_x(i_s - 1, j_m, \tau) \frac{h(i_m, j_m, \tau - 1) - h(i_m - 1, j_m, \tau - 1)}{\Delta\xi} \quad \text{if } v_x(i_m, j_m, \tau) > 0 \\
&+ v_x(i_s, j_m, \tau) \frac{h(i_m + 1, j_m, \tau - 1) - h(i_m, j_m, \tau - 1)}{\Delta\xi} \quad \text{if } v_x(i_m, j_m, \tau) < 0 \\
&+ v_y(i_m, j_s - 1, \tau) \frac{h(i_m, j_m, \tau - 1) - h(i_m, j_m - 1, \tau - 1)}{\Delta\eta} \quad \text{if } v_y(i_m, j_m, \tau) > 0 \\
&+ v_y(i_m, j_s, \tau) \frac{h(i_m, j_m + 1, \tau - 1) - h(i_m, j_m, \tau - 1)}{\Delta\eta} \quad \text{if } v_y(i_m, j_m, \tau) < 0 \\
&- v_z(i_m, j_m, \tau) = a^\perp(i_m, j_m, \tau),
\end{aligned} \tag{57}$$

where  $k = \text{KMAX}$  everywhere. For simplicity we now drop all indices except those that differ from  $(i_m, j_m, \tau)$  and obtain the explicit formula for  $h(\tau)$ :

$$\begin{aligned}
h(\tau) = & h(\tau - \Delta\tau) + \Delta\tau \left( a^\perp + v_z \right. \\
& - v_x(i_s - 1) \frac{h(\tau - 1) - h(i_m - 1, \tau - 1)}{\Delta\xi} \quad \text{if } v_x(i_m) > 0 \\
& - v_x(i_s) \frac{h(i_m + 1, \tau - 1) - h(\tau - 1)}{\Delta\xi} \quad \text{if } v_x(i_m) < 0 \\
& - v_y(j_s - 1) \frac{h(\tau - 1) - h(j_m - 1, \tau - 1)}{\Delta\eta} \quad \text{if } v_y(j_m) > 0 \\
& \left. - v_y(j_s) \frac{h(j_m + 1, \tau - 1) - h(\tau - 1)}{\Delta\eta} \quad \text{if } v_y(j_m) < 0 \right). \tag{58}
\end{aligned}$$

## 5 The SIA algorithm

### 5.1 The existing SIA algorithm

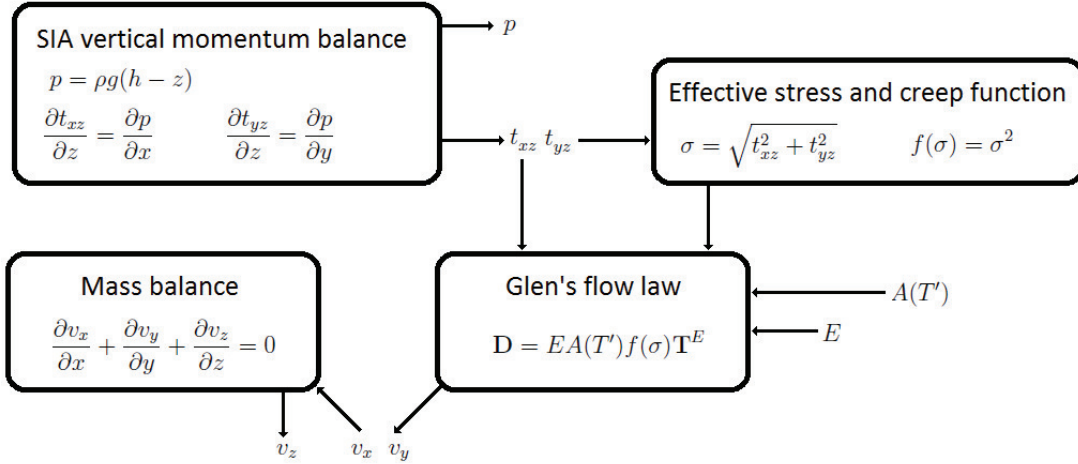


Figure 6: The structure of the existing SIA algorithm

The existing SIA algorithm computes stresses, pressures and velocities of an example ice sheet of fixed geometry. The derivation of the equations for the vertical momentum balance is not shown here but can be found in [4].

Pressure and shear stresses in the horizontal plane depend entirely on the geometry of the ice. The shear stresses are used to calculate the effective shear stress and creep function, which are needed in Glen's flow law together with the shear stresses themselves. Glen's flow law is used to compute horizontal velocities with a constant ratefactor  $A(T')$  of  $3.169 \cdot 10^{-24} \text{ s}^{-1} \text{ Pa}^{-3}$ , which corresponds to a pressure melting point corrected temperature of  $-2^\circ\text{C}$ . The mass balance is finally used to obtain the vertical velocities.  $E$  is the enhancement factor.

In this algorithm steady-state conditions are assumed and there is no time dependency.

## 5.2 New algorithm with temperature implemented

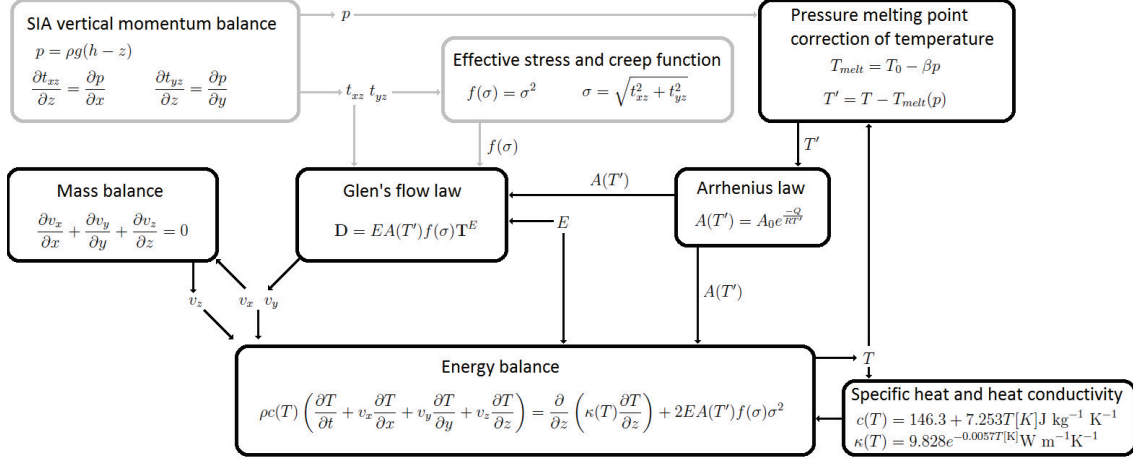


Figure 7: The structure of the temperature-dependent SIA algorithm. The gray parts receive no feedback from the temperature and do not change with time

Introducing temperature variations permits using a temperature dependent ratefactor, which in its turn affects stresses, velocities and pressures, see Figure 7. The temperature and pressure are used to compute the pressure melting point corrected temperature, which is used in Arrhenius law to obtain the temperature-dependent ratefactor, which in its turn affects the velocity computations. The temperature itself depends on velocities, the ratefactor, the enhancement factor, the specific heat and the heat conductivity. Note that in SIA the temperature does not affect the shear stresses when the geometry of the ice is held fixed.

With the energy equation a time dependency is introduced in the problem, which makes it necessary to introduce initial values. Velocities, stresses and pressures are initially set to zero as they do not depend directly on previous time steps.

## 5.3 New algorithm with temperature and free surface evolution implemented

When evolution of the free surface is implemented the model becomes fully transient as the ice thickness affects the vertical momentum balance and thus gives feedback to all parts of the model as shown in Figure 8.

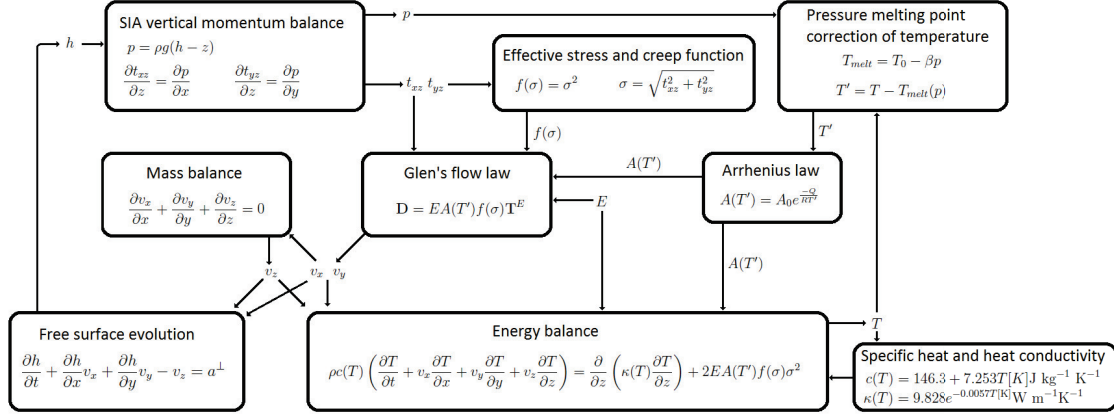


Figure 8: The structure of the transient SIA algorithm with both temperature and evolution of the free surface

## 6 Method for comparison with ElmerIce

### 6.1 About ElmerIce

Elmer is an open source multi-physical simulation software which solves problems described by partial differential equations using the finite element method, [8]. ElmerIce builds on Elmer but also includes developments related to glaciological problems. With ElmerIce it is possible to solve the full Stokes equations for limited problems. In order to run ElmerIce one first needs to define a grid and create an input file. The input file contains material properties, boundary conditions, initial conditions, simulation options such as number and size of time steps and also specifies what solvers are to be used, that is, which physical processes that are to be taken into consideration and how these equations are to be solved. In this project the Stokes solver was used to compute the flow solution, the temperate ice and deformational heat solvers were used to generate the temperature field and the free surface and mesh update solvers were used to compute the changing geometry. Note that despite the name, the temperate ice solver is not specific for temperate ice. The full input file is given in Appendix A.

### 6.2 Test problem

In order to evaluate how well the new SIA algorithm approximates the Stokes equations a test problem was solved on the one hand with the Matlab implementation of SIA and on the other hand with ElmerIce, and the results were compared. The test problem is a simple ice sheet on a base with the shape of a smooth, gently sloping sinus wave as depicted in Figure 3. The problem is two-dimensional, and the horizontal extent  $L$  of the ice sheet can be varied. When comparing different  $L$  the SIA scaling requires that the slope is arctane in order to give comparable results, [2]. However, as the obtained velocities increase with the slope it may also be meaningful to compare results of different  $L$  with the same slope.

The choice of boundary conditions and initial conditions was done in a way that would generate an ice sheet that would never reach melting temperatures, as the model is only valid for cold ice. To achieve this, the surface temperature was set

to a constant  $-25^{\circ}\text{C}$  and the geothermal heat flow to  $0.03\text{mW}/\text{m}^2$  which is a low but realistic value, [6]. It was noted that the temperature change due to friction is almost negligible compared to the effect of the geothermal heat flow. For simplicity the initial temperature is set to  $-25^{\circ}\text{C}$  throughout the ice and the accumulation-ablation function to zero. The boundary conditions on the vertical boundaries are made periodic, so that values obtained furthest out in the flow direction is copied to the upstream boundary.

### 6.3 Grid resolution and time step for SIA

Appropriate grid resolution and time step were determined by a trial-and-error approach where the SIA model was run with different grids and time steps. The results were firstly examined so that no unexplained weirdnesses occur such as unrealistic patterns or behavior like oscillations in time of different variables that would indicate instability. It was found that a coarser horizontal grid could tolerate longer time steps, while a fine grid required smaller time steps in order to be stable.

Secondly the results were compared to the results of finer and coarser discretization to get an indication of how the accuracy was affected. The choice was made so that the result would not change significantly for a finer discretization.

A grid with  $\Delta x = 8\text{km}$ ,  $\Delta z \approx 30\text{m}$  (30 elements in vertical direction) and a time step of 100 years was finally chosen. Graphs with comparison of results of finer and coarser discretizations are found in Appendix B.

### 6.4 Grid resolution and time step for ElmerIce

As for SIA, the appropriate grid resolution and time step were selected for ElmerIce by a trial-and-error method, where results of a simulation over 1000 years were compared for different grids and time steps. The grid that was chosen has  $\Delta x = 1.6\text{km}$  and is the finest one that was tested, as a finer grid would result in too long computation times. Compared to a grid with  $\Delta x = 6.4\text{km}$  the velocities are not much affected by the finer discretization, though the temperature change slows down for the finer grid. In the vertical direction the grid is identical to the grid used in SIA in order to obtain identical observation points for comparison between the two models. A time step size of  $\Delta t = 50$  years was used and found sufficiently small as a comparison of results to a run with  $\Delta t = 20$  years showed hardly any difference at all.

Graphs with comparison of results of different discretizations are found in Appendix C.

## 7 Results

In order to investigate how well SIA approximates the Stokes equations for the test problem described in Section 6.2 the results of a simulation over 10 000 years was compared to an ElmerIce solution. For the comparison the velocities and temperatures of nine locations in the ice were plotted over time - three points over the bump, three points over the pit and three points over the slope in the center of the ice. The comparison was done for three different setups: One with aspect ratio  $\epsilon = 1/160 = 6.25 * 10^{-3}$  and  $\alpha = \arctan \epsilon$ , one with  $\epsilon = 1/1280 = 7.8 * 10^{-4}$  and

$\alpha = \arctan \epsilon$  and a third with  $\epsilon = 1/160 = 6.25 * 10^{-3}$  and  $\alpha = \arctan 1/1280$ , that is, a large aspect ratio but with a small slope. The aspect ratios of real terrestrial ice sheets are around  $10^{-2} - 10^{-3}$  [?]. The slope varies greatly but both the slopes used in this project are within a realistic interval, [7]. Finally the resulting temperature and velocity fields of the run with the small aspect ratio are presented.

## 7.1 Comparison with ElmerIce with large aspect ratio

Figures 10-13 compare the results of SIA and Elmer for a simulation with  $\epsilon = 6.25 * 10^{-3}$  and  $\alpha = \arctan \epsilon$ . The development of temperature and velocities in the points shown in Figure 9 is compared. As shown in Figure 10 the temperatures agree very well, though there is a small tendency that the Elmer temperature changes faster than the SIA temperature. The horizontal velocities shown in Figure 11 differ more and most clearly in the points most to the left which are located right over the bump. Note that the scale of the y-axis differ between the different plots. The vertical velocities in Figure 12 also disagree most in these points and agree well in the central points. Figure 13 shows the final geometry. The computed change is greater in SIA than in Elmer, but the shape of the new surface is the same. The SIA surface bends down towards the left boundary in a way that the Elmer surface does not, but this apparent difference is probably due to the much coarser spatial discretization in SIA.

## 7.2 Comparison with ElmerIce with small aspect ratio

Figures 15-19 compare the results of SIA and Elmer for a simulation with  $\epsilon = 7.8 * 10^{-4}$ . The development of temperature and velocities in the points shown in Figure 14 is compared. Figure 15 shows that the temperature development agrees very well between the two models. Figure 16 shows the development of the horizontal velocities, which also agrees fairly well. The vertical velocities presented in Figure 17 differ significantly in two of the observation points while the rest agree well. The geometry does not change much over the simulated time as can be seen in Figure 18, but the closeup in Figure 19 show that the two models agree well even on such a small displacement as 0.2m.

## 7.3 Comparison with ElmerIce with large aspect ratio and small slope

The results of the setup with  $\epsilon = 6.25 * 10^{-3}$  and a slope of  $\alpha = \arctan 1/1280$  (corresponding to  $\epsilon = 7.8 * 10^{-4}$ ) are presented in Figures 21-25 and the points that are compared are presented in Figure 20. As in both the previous setups the temperature agrees well, Figure 21. The horizontal velocities, Figure 22, differ a little bit but not significantly more than in the setup with small aspect ratio and identical slope, and the vertical velocities, Figure 23, even seem to agree slightly better in the observed points for this run than for the one with smaller aspect ratio. The surface, Figures 24-25 is also similar to the run with smaller aspect ratio.

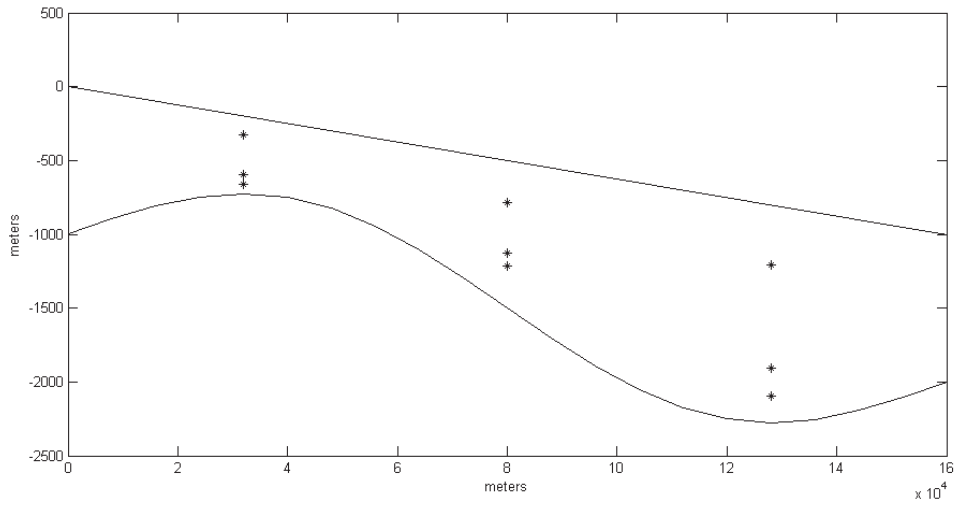


Figure 9: Observation points for comparison between SIA and ElmerIce

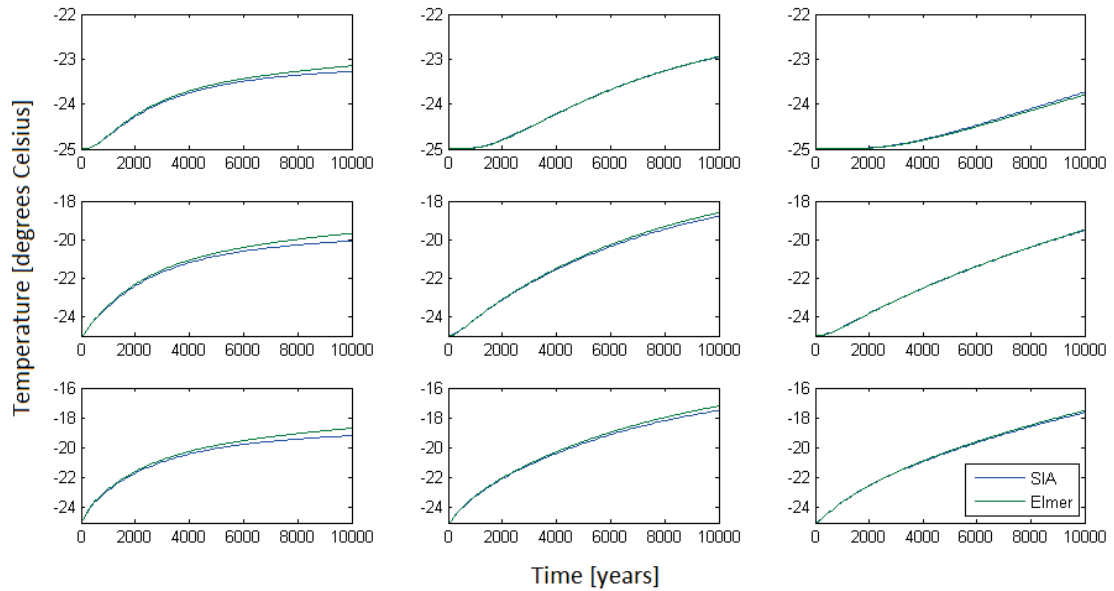


Figure 10: Temperature development over 10 000 years with  $\epsilon = 6.25 \times 10^{-3}$ . The locations of the observation points are shown in Figure 9.

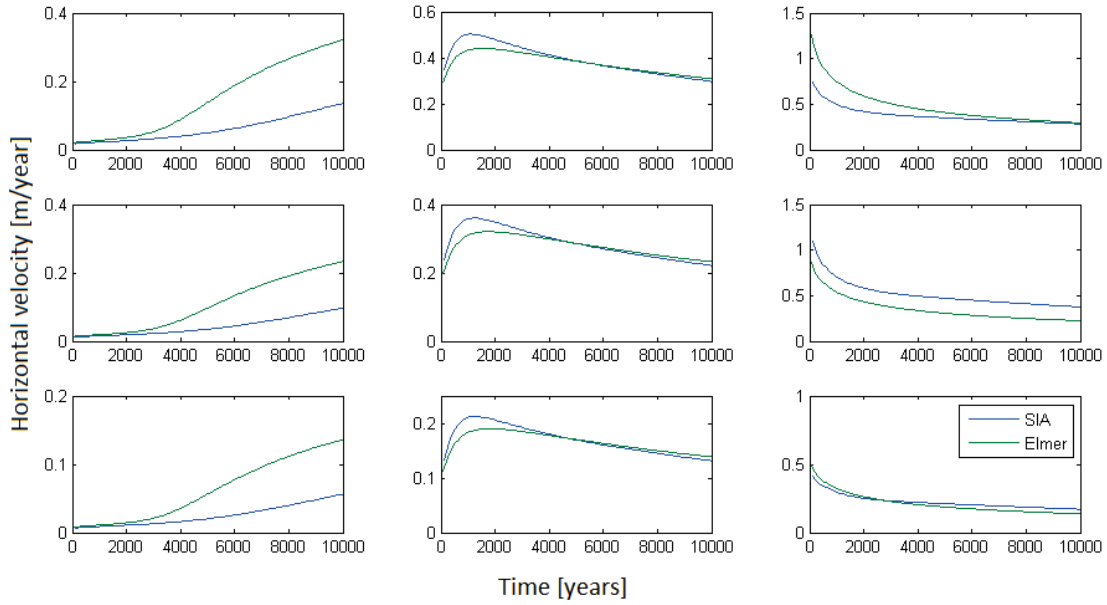


Figure 11: Horizontal velocity development over 10 000 years with  $\epsilon = 6.25 \times 10^{-3}$ . The locations of the observation points are shown in Figure 9.

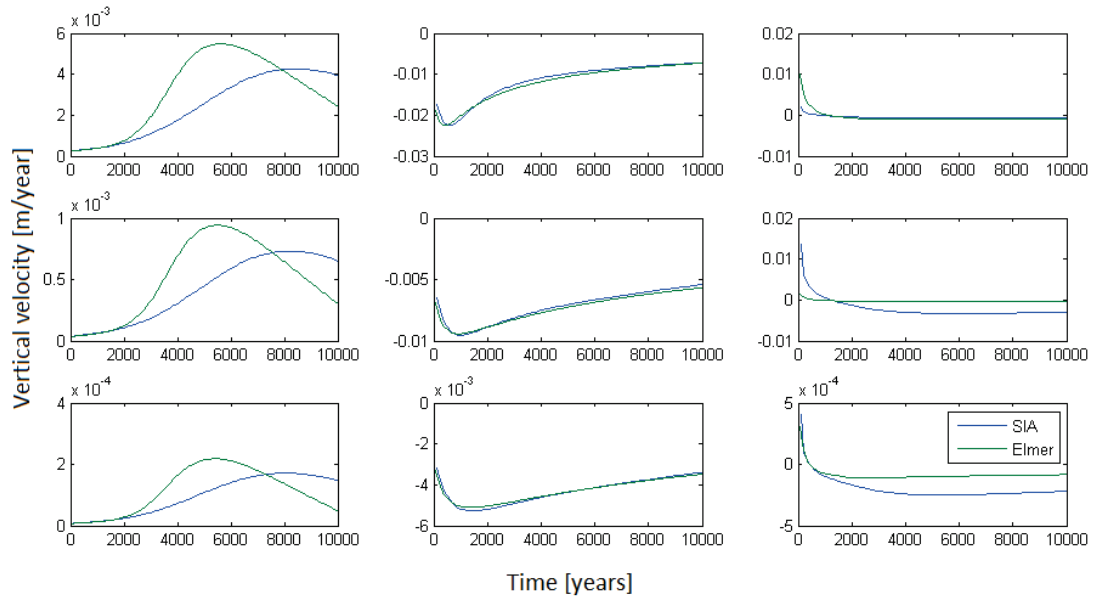


Figure 12: Vertical velocity development over 10 000 years with  $\epsilon = 6.25 \times 10^{-3}$ . The locations of the observation points are shown in Figure 9.

## 7.4 Temperature and velocity fields in SIA after 10 000 years

Figures 26-28 present the temperature field, horizontal velocity field and vertical velocity field for the test problem with aspect ratio  $\epsilon = 7.8 * 10^{-4}$  and  $\alpha = \arctan \epsilon$  after 10 000 years. The temperature, Figure 26, is highest at the base and the temperature decreases towards the surface. The horizontal velocity, Figure 27, is highest on the part where the ice thickness is greatest and closer to the surface, everywhere moving in positive direction (to the right in the figure). The vertical velocity, Figure 28, reaches its highest (absolute) values in the same region, with negative velocities where the ice is moving down in the pit and positive velocities where it is pushed up again.

## 8 Discussion and conclusions

In this project equations for temperature and free surface development were implemented in a Matlab version of the Shallow Ice Approximation (SIA). SIA is an approximation of the full Stokes equations which is valid for small aspect ratios.

The code produced in this project approximates the Stokes equations well for an aspect ratio of  $\epsilon = 7.8 * 10^{-4}$  and a slope of  $\alpha = \arctan \epsilon$ . For these settings all compared parameters agree well except for the vertical velocity in the two uppermost points in the pit. This could be due to large local variations in vertical velocity at these points as they are located between the fields of downward and upward flow.

When the slope was kept at  $\alpha = \arctan \epsilon$  the approximation was improved for a smaller aspect ratio as would be expected for the Shallow Ice Approximation. However, the results were improved as much by simply decreasing the slope without decreasing the aspect ratio. There is no apparent difference between different aspect ratios with the same slope. While both the compared slopes are realistic for real ice sheets, terrestrial ice sheets do not normally have aspect ratios below  $10^{-3}$ .

Both the temperature equation and the free surface equation which were implemented in this project seem to be less sensitive to slope and aspect ratio than the velocity calculations and work well even at an aspect ratio of  $\epsilon = 6.25 * 10^{-3}$ . This indicates that it might be useful to combine more accurate higher order solutions for stresses and velocities with temperatures and surface computed by the SIA equations.

## References

- [1] J. Ahlkrona. Implementing higher order dynamics into the ice sheet model SICOPOLIS. Master's thesis, Department of Information Technology, Uppsala University, 2011.
- [2] J. Ahlkrona, N. Kirchner, and P. Lötstedt. A numerical study of scaling relations for non-newtonian thin film flows with applications in ice sheet modelling. *Quart. J. Mech. Appl. Math.*, Accepted for publication 2013.
- [3] D. R. Baral, K. Hutter, and R. Greve. Asymptotic theories of large-scale motion, temperature and moisture distribution in land-based polythermal ice sheets: A critical review and new developments. *Applied Mechanics Reviews*, 54(3):215–256, 2001.
- [4] R. Greve and H. Blatter. *Dynamics of Ice Sheets and Glaciers*. Advances in Geophysical and Environmental Mechanics and Mathematics (AGEM<sup>2</sup>), Springer, Berlin, 2009.
- [5] W.S.B. Paterson. *The Physics of Glaciers*. Pergamon Press, Oxford, 1994.
- [6] D. Pollard, R. M. DeConto, and A. A. Nyblade. Sensitivity of Cenozoic Antarctic ice sheet variations to geothermal heat flux. *Global and Planetary Change*, 49:63–74, 2005.
- [7] The National Snow and Ice Data Center (NSIDC). Atlas of the cryosphere. [http://nsidc.org/data/atlas/news/bedrock\\_elevation.html](http://nsidc.org/data/atlas/news/bedrock_elevation.html), May 2013.
- [8] Elmer website. <http://www.csc.fi/english/pages/elmer>, May 2013.

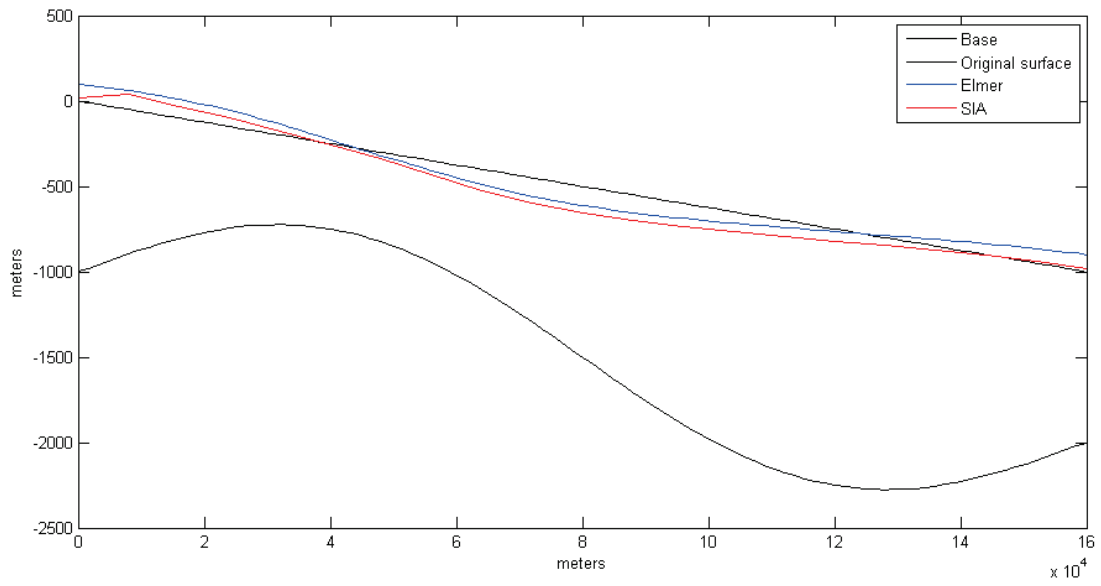


Figure 13: Geometry after 10 000 years with  $\epsilon = 6.25 * 10^{-3}$

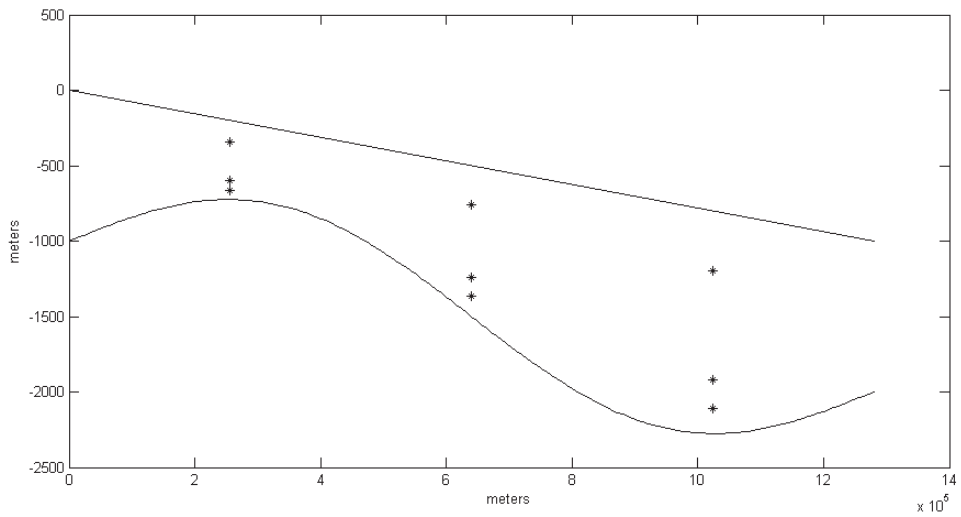


Figure 14: Observation points for comparison between SIA and ElmerIce

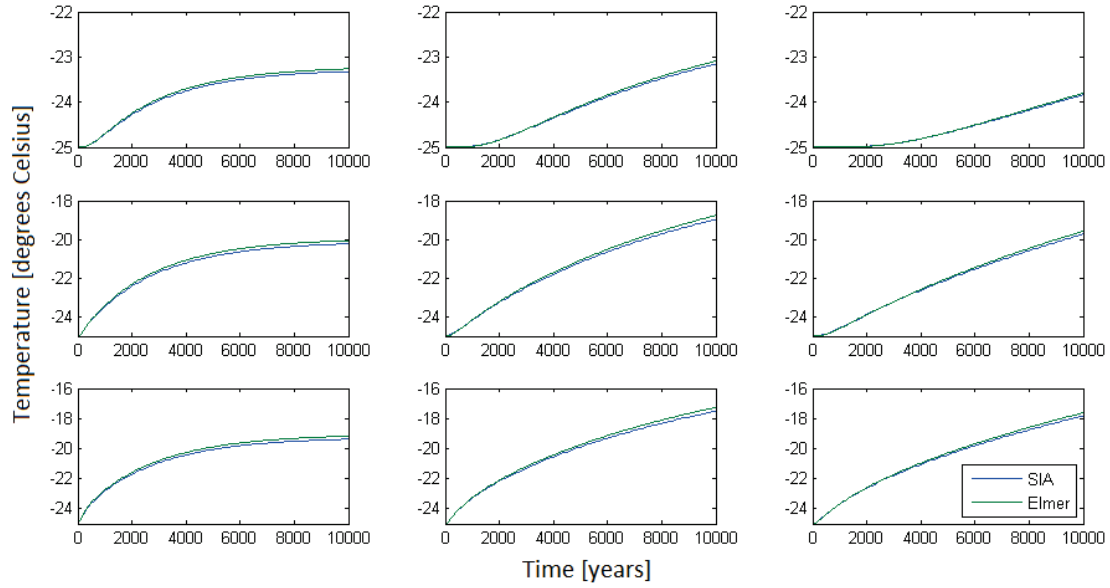


Figure 15: Temperature development over 10000 years with  $\epsilon = 7.8 \cdot 10^{-4}$ . The locations of the observation points are shown in Figure 14.

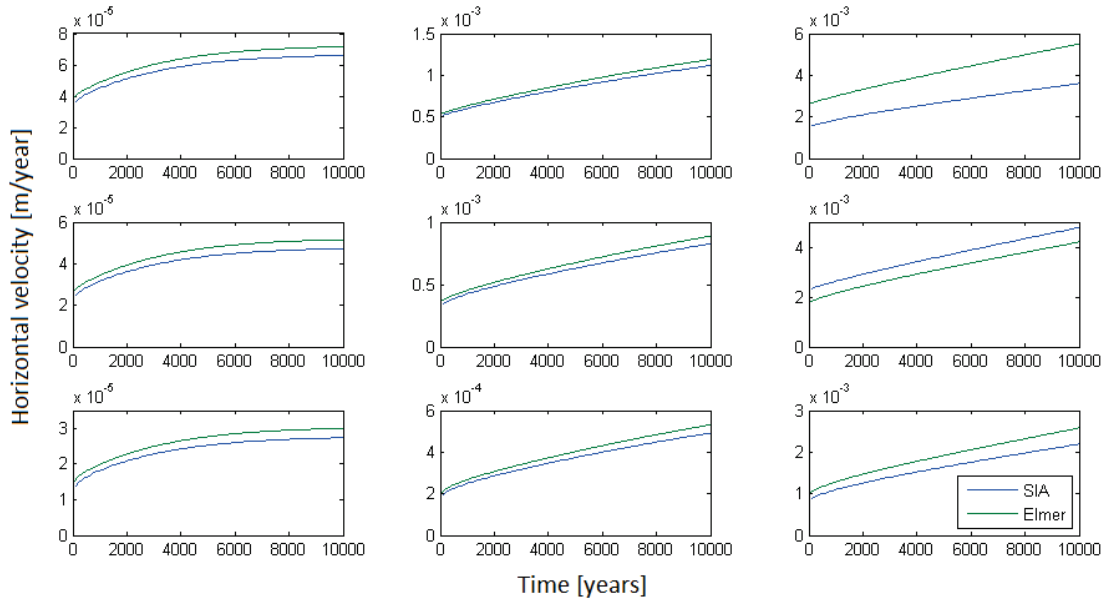


Figure 16: Horizontal velocity development over 10000 years with  $\epsilon = 7.8 \cdot 10^{-4}$ . The locations of the observation points are shown in Figure 14.

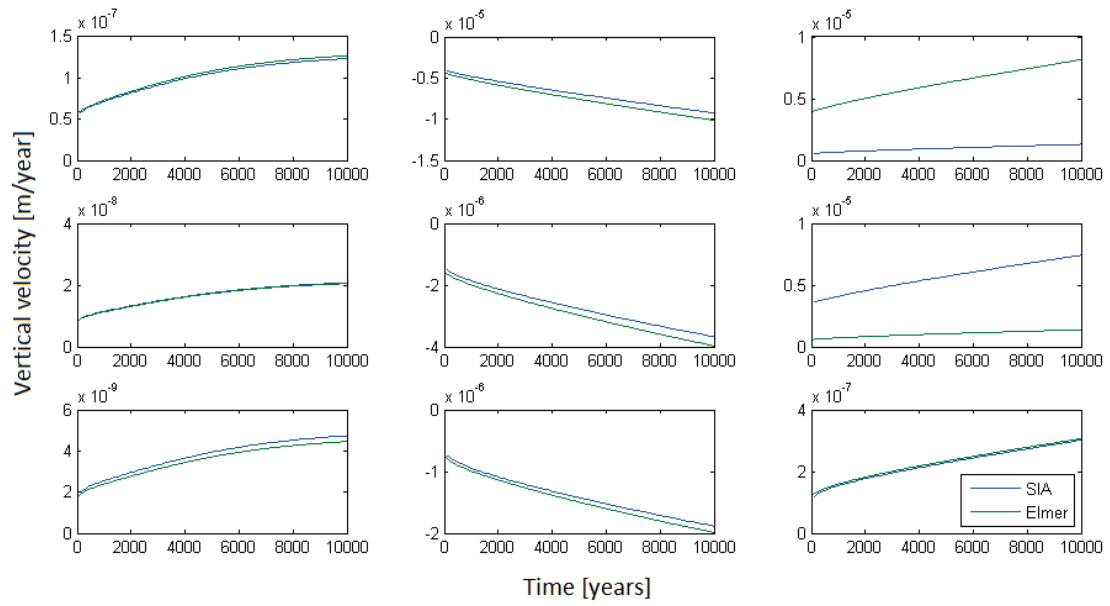


Figure 17: Vertical velocity development over 10000 years with  $\epsilon = 7.8 \times 10^{-4}$ . The locations of the observation points are shown in Figure 14.

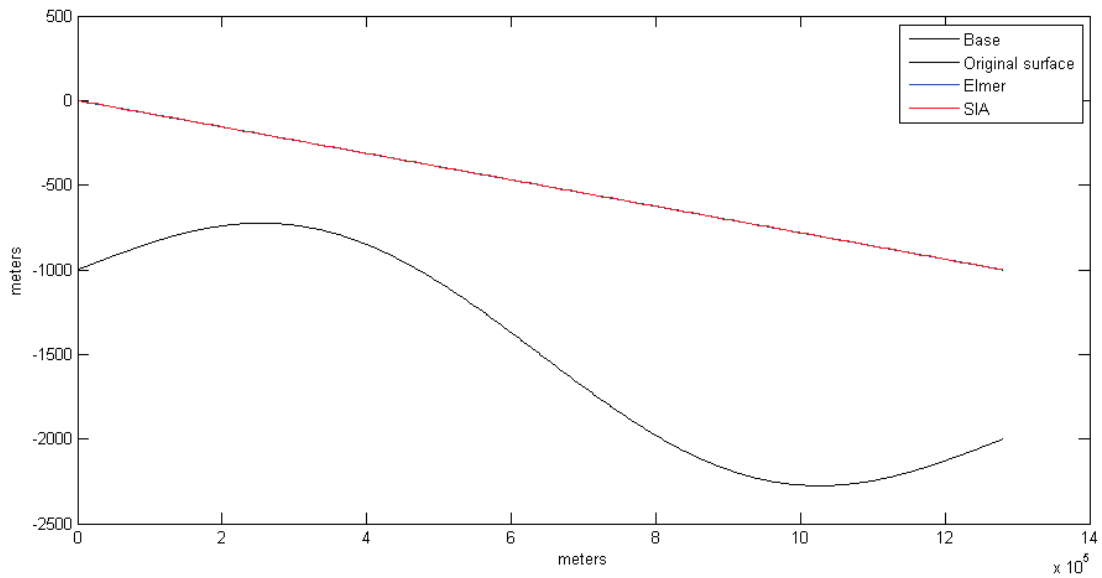


Figure 18: Geometry after 10000 years with  $\epsilon = 7.8 \times 10^{-4}$

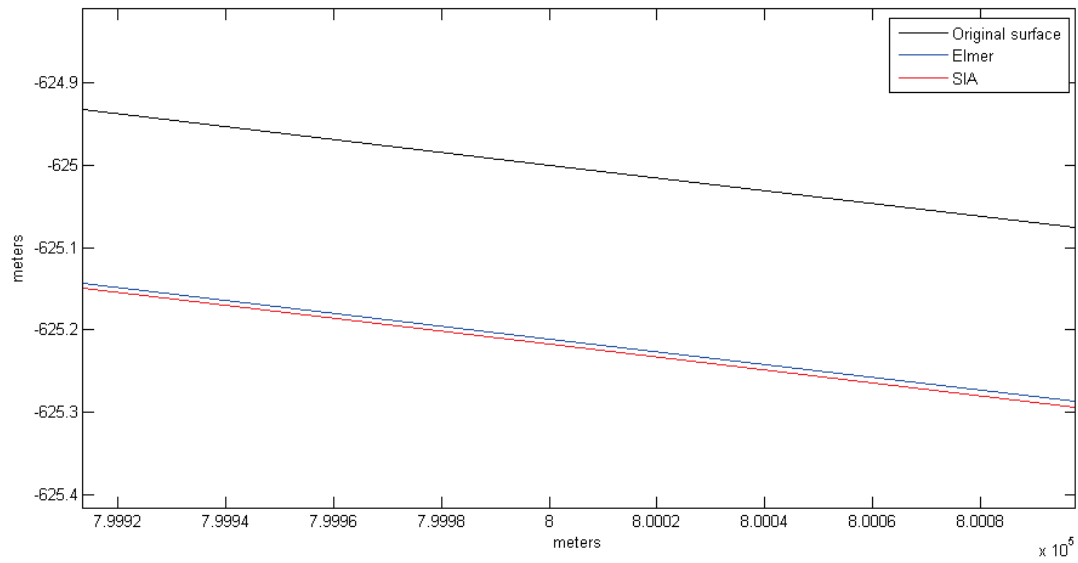


Figure 19: Closeup on surface with  $\epsilon = 7.8 * 10^{-4}$

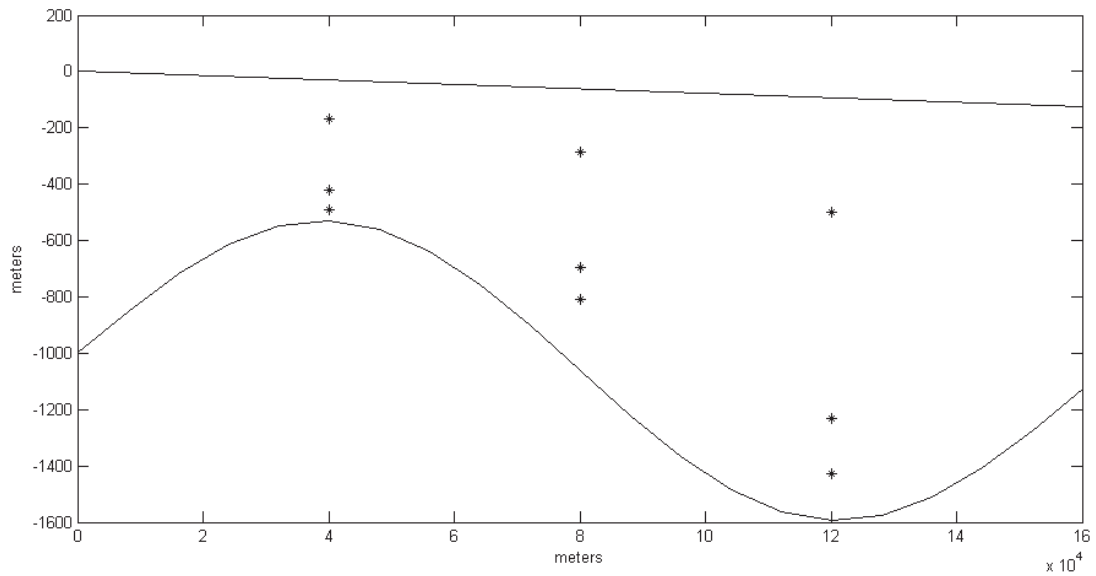


Figure 20: Observation points for comparison between SIA and ElmerIce with  $\epsilon = 6.25 * 10^{-3}$  and small slope

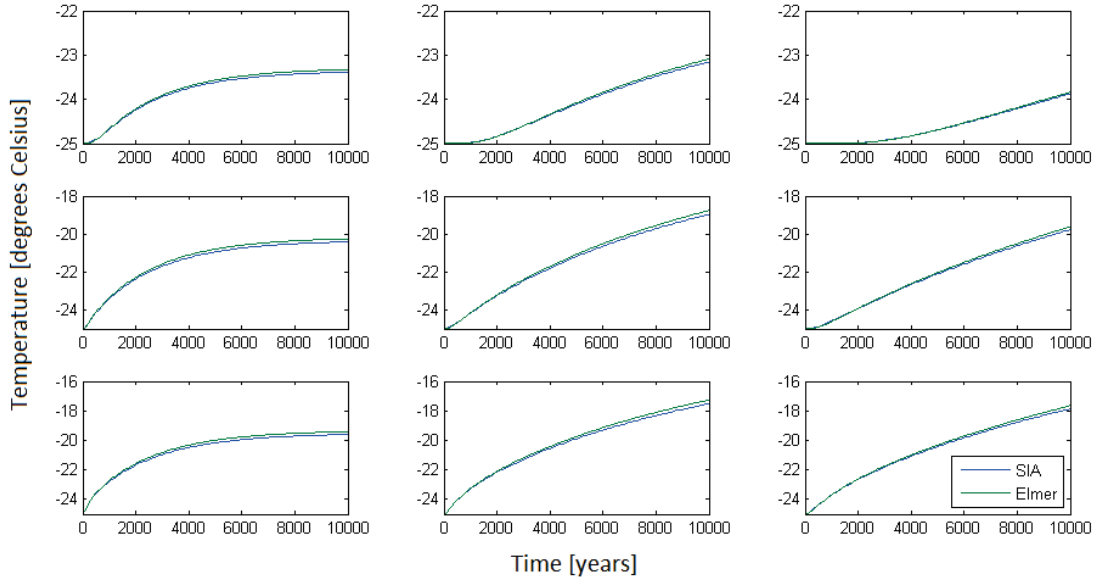


Figure 21: Temperature development over 10000 years with  $\epsilon = 6.25 \times 10^{-3}$  and small slope. The locations of the observation points are shown in Figure 20.

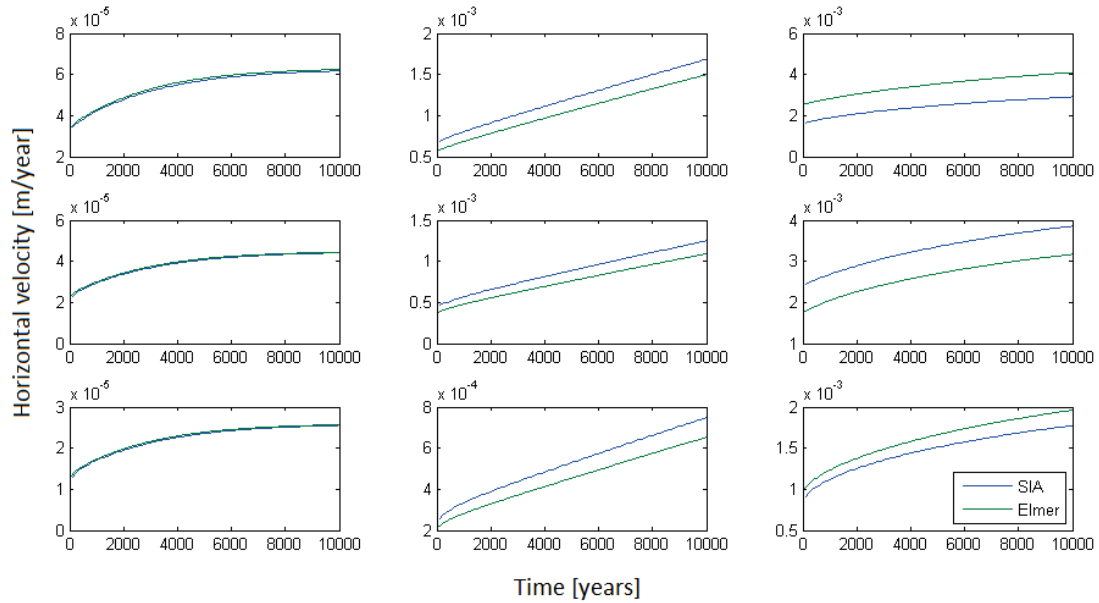


Figure 22: Horizontal velocity development over 10000 years with  $\epsilon = 6.25 \times 10^{-3}$  and small slope. The locations of the observation points are shown in Figure 20.

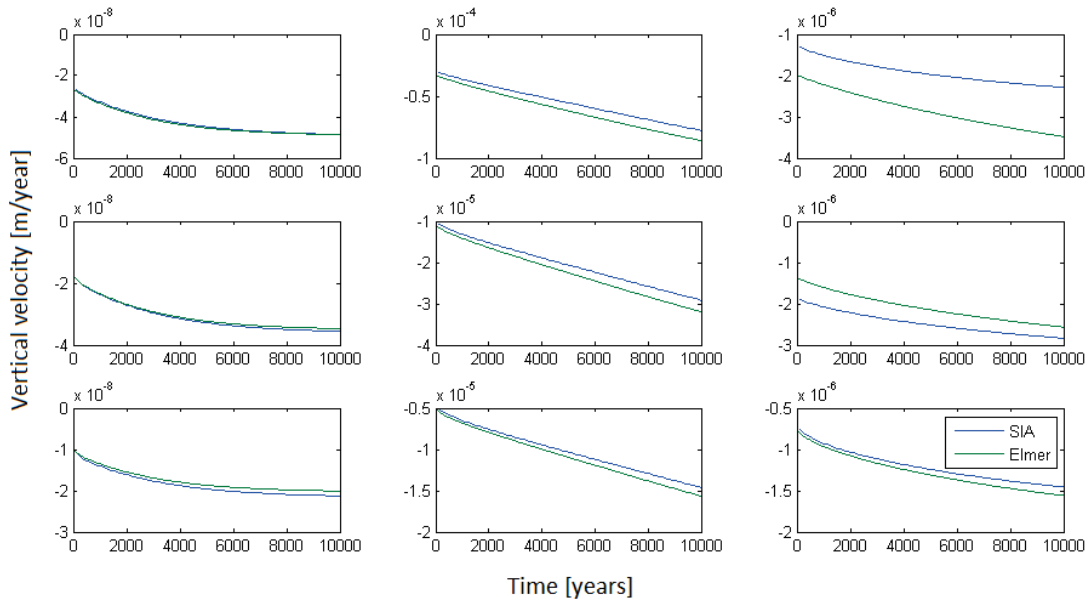


Figure 23: Vertical velocity development over 10000 years with  $\epsilon = 6.25 \times 10^{-3}$  and small slope. The locations of the observation points are shown in Figure 20.

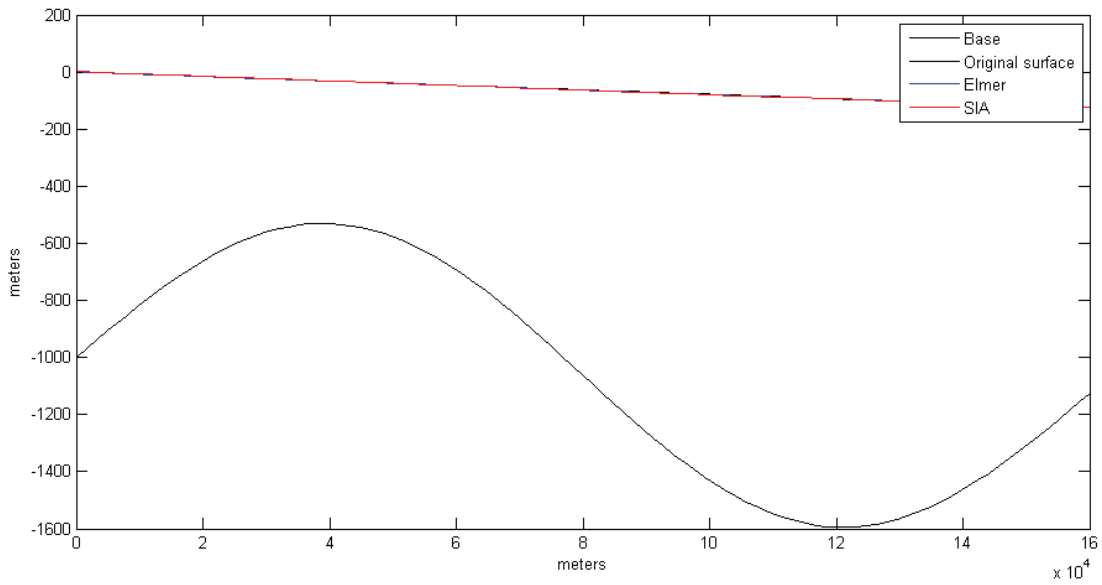


Figure 24: Geometry after 10000 years with  $\epsilon = 6.25 \times 10^{-3}$  and small slope

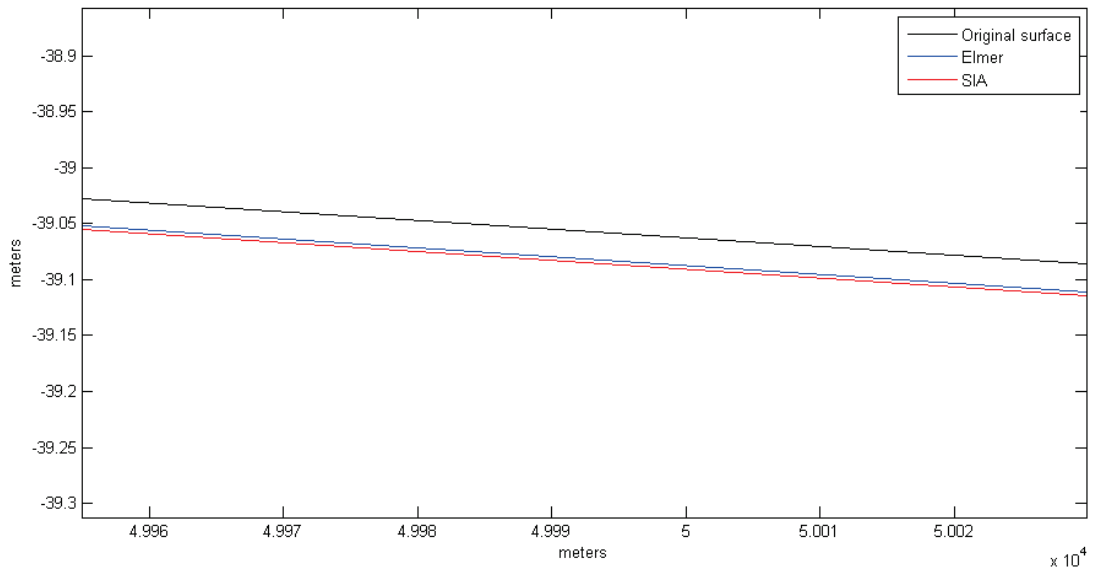


Figure 25: Closeup on surface with  $\epsilon = 6.25 * 10^{-3}$  and small slope

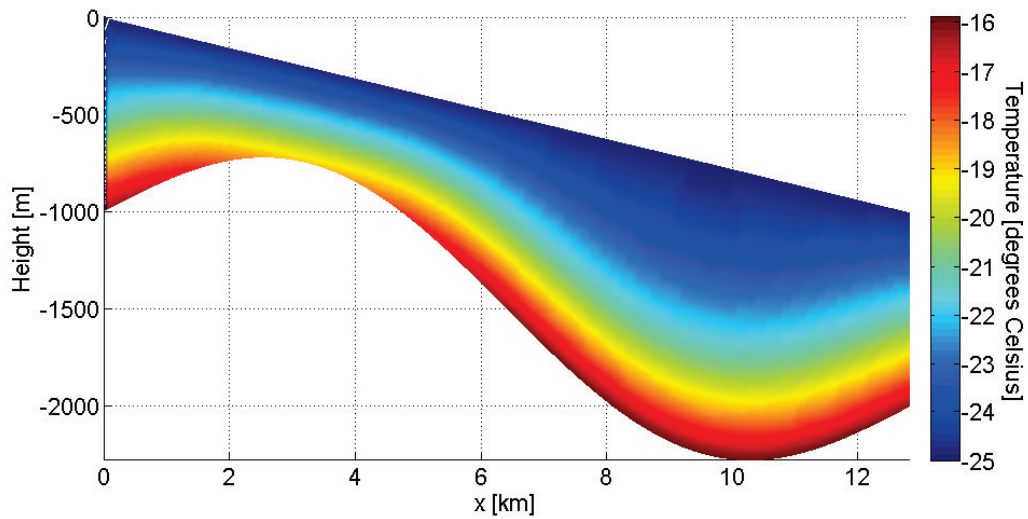


Figure 26: Temperature field after 10000 years with  $\epsilon = 7.8 * 10^{-4}$

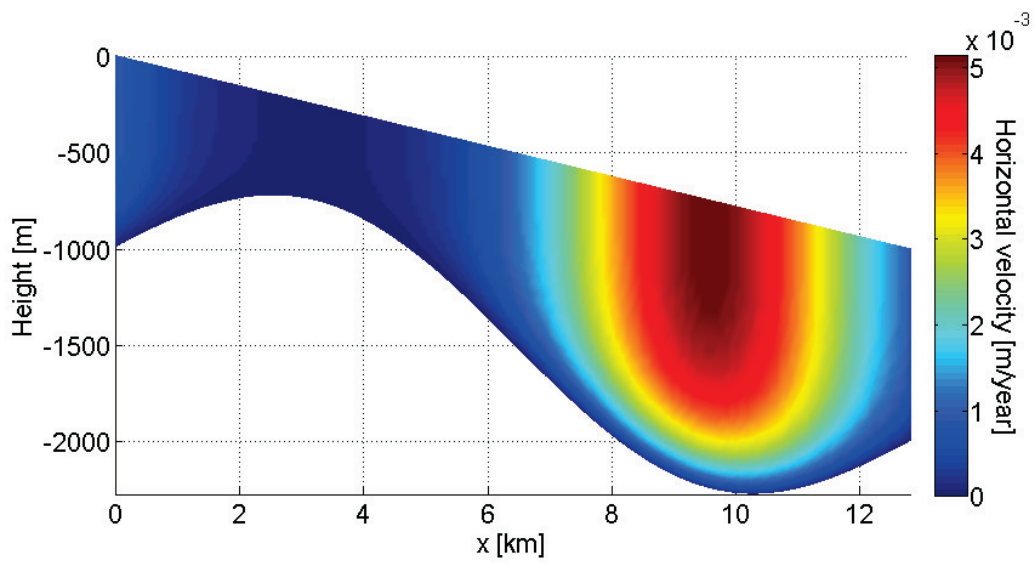


Figure 27: Horizontal velocity field after 10000 years with  $\epsilon = 7.8 \times 10^{-4}$

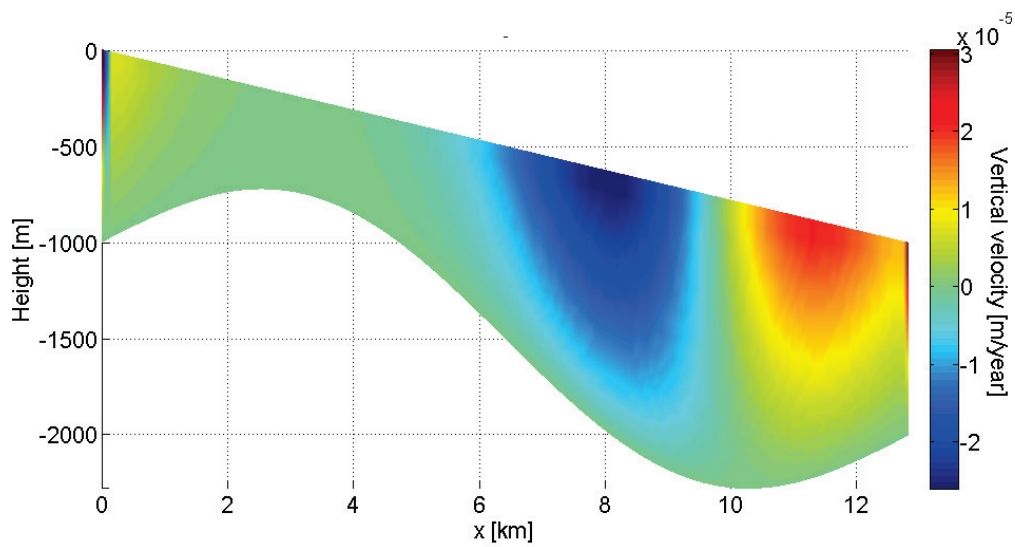


Figure 28: Vertical velocity field after 10000 years with  $\epsilon = 7.8 \times 10^{-4}$